

# Magnesium and iron isotopes in 2.7 Ga Alexo komatiites: Mantle signatures, no evidence for Soret diffusion, and identification of diffusive transport in zoned olivine

Nicolas Dauphas<sup>a,\*</sup>, Fang-Zhen Teng<sup>b</sup>, Nicholas T. Arndt<sup>c</sup>

<sup>a</sup> *Origins Laboratory, Department of the Geophysical Sciences and Enrico Fermi Institute, The University of Chicago,  
5734 South Ellis Avenue, Chicago IL 60637, USA*

<sup>b</sup> *Isotope laboratory, Department of Geosciences and Arkansas Center for Space and Planetary Sciences, University of Arkansas,  
Fayetteville, AR 72701, USA*

<sup>c</sup> *LGCA, UMR 5025 CNRS, Université Joseph Fourier à Grenoble, BP53, 38041 Grenoble Cedex, France*

Received 28 July 2009; accepted in revised form 26 February 2010; available online 3 March 2010

## Abstract

Komatiites from Alexo, Canada, are well preserved and represent high-degree partial mantle melts (~50%). They are thus well suited for investigating the Mg and Fe isotopic compositions of the Archean mantle and the conditions of magmatic differentiation in komatiitic lavas. High precision Mg and Fe isotopic analyses of 22 samples taken along a 15-m depth profile in a komatiite flow are reported. The  $\delta^{25}\text{Mg}$  and  $\delta^{26}\text{Mg}$  values of the bulk flow are  $-0.138 \pm 0.021\text{‰}$  and  $-0.275 \pm 0.042\text{‰}$ , respectively. These values are indistinguishable from those measured in mantle peridotites and chondrites, and represent the best estimate of the composition of the silicate Earth from analysis of volcanic rocks. Excluding the samples affected by secondary Fe mobilization, the  $\delta^{56}\text{Fe}$  and  $\delta^{57}\text{Fe}$  values of the bulk flow are  $+0.044 \pm 0.030\text{‰}$ , and  $+0.059 \pm 0.044\text{‰}$ , respectively. These values are consistent with a near-chondritic Fe isotopic composition of the silicate Earth and minor fractionation during komatiite magma genesis. In order to explain the early crystallization of pigeonite relative to augite in slowly cooled spinifex lavas, it was suggested that magmas trapped in the crystal mush during spinifex growth differentiated by Soret effect, which should be associated with large and coupled variations in the isotopic compositions of Mg and Fe. The lack of variations in Mg and Fe isotopic ratios either rules out the Soret effect in the komatiite flow or the effect is effaced as the solidification front migrates downward through the flow crust. Olivine separated from a cumulate sample has light  $\delta^{56}\text{Fe}$  and slightly heavy  $\delta^{26}\text{Mg}$  values relative to the bulk flow, which modeling shows can be explained by kinetic isotope fractionation associated with Fe–Mg inter-diffusion in olivine. Such variations can be used to identify diffusive processes involved in the formation of zoned minerals.

© 2010 Elsevier Ltd. All rights reserved.

## 1. INTRODUCTION

Initial studies of magnesium and iron isotopic variations in natural materials focused on processes occurring in low-temperature aqueous environments, or involving high temperature chemistry between gas and condensed phases in the protosolar nebula (Young and Galy, 2004; Dauphas

and Rouxel, 2006, and references therein). Improvements in precision revealed that Fe isotopes could also be fractionated during high temperature igneous processes like mantle metasomatism, partial melting, fractional crystallization, and fluid exsolution (Beard and Johnson, 2004, 2007; Williams et al., 2004, 2005; Poitrasson and Freyrier, 2005; Weyer et al., 2005; Schoenberg and von Blanckenburg, 2006; Weyer and Ionov, 2007; Heimann et al. 2008; Teng et al., 2008; Schoenberg et al., 2009; Schuessler et al., 2009; Dauphas et al., 2009a). Although not documented in nature, chemical and thermal diffusion in silicate

\* Corresponding author. Tel.: +1 773 702 2930.  
E-mail address: [dauphas@uchicago.edu](mailto:dauphas@uchicago.edu) (N. Dauphas).

melts can also fractionate Mg and Fe isotopes (Richter et al., 2008, 2009a,b; Huang et al., 2009). The Mg and Fe isotopic compositions of the bulk silicate Earth (BSE) and the mechanism governing Fe isotopic fractionation during partial melting are not fully resolved (Weyer et al., 2005, 2007; Schoenberg and von Blanckenburg, 2006; Weyer and Ionov, 2007; Beard and Johnson, 2007; Poitrasson, 2007; Wiechert and Halliday, 2007; Teng et al., 2007; Dauphas et al., 2009a; Handler et al., 2009). Several studies have shown that on average, fertile peridotites have chondritic Mg and Fe isotopic compositions (Weyer et al., 2005; Schoenberg and von Blanckenburg, 2006; Weyer and Ionov, 2007; Handler et al., 2009). Terrestrial basalts also have chondritic Mg isotopic composition (Teng et al., 2007, 2010). A source of contention has been the significance of the heavy Fe isotopic compositions measured in mid-ocean ridge and oceanic island basalts (MORB and OIB, respectively). The finding that boninites and some island arc basalts (IAB) have near-chondritic Fe isotopic compositions supports the view that the BSE has chondritic composition and that the heavy composition of oceanic basalts relative to the mantle reflects redox-controlled Fe isotopic fractionation during partial melting (Dauphas et al., 2009a).

Komatiites have several characteristics that make them particularly useful for addressing questions relevant to mantle melting and non-traditional stable isotope geochemistry. These ultramafic magmas represent very high degree partial melts (Herzberg, 1992; Arndt, 2003). Even if isotopic fractionation was present between melt and solid, the composition of the melt approaches that of the initial solid as the degree of partial melting increases. Komatiites are thought to form in a plume that was hotter than the surrounding mantle (e.g., Arndt et al., 1998), which was itself hotter than the modern mantle due to secular cooling of the Earth (Nisbet et al., 1993; Herzberg et al., 2007). Any equilibrium isotopic fractionation should be reduced at these high temperatures ( $\propto 1/T^2$ ). When they formed, komatiites had near-neutral buoyancy (Ohtani, 1984; Miller et al., 1991). This, together with fast diffusion at high temperature should eliminate kinetic isotope effects. All these aspects concur to mitigate isotopic fractionation between mantle and komatiite melts, making these samples ideal for studying the Mg and Fe isotopic compositions of deep-seated mantle sources.

Komatiites flows at Alexo, Ontario, Canada, show clear evidence for magmatic evolution driven by olivine accumulation (Arndt, 1986). This is similar to the Kilauea Iki lava lake, where Teng et al. (2008) reported significant Fe isotopic fractionation. The underlying mechanism for such fractionation is poorly understood. If it is associated with different partitioning of ferrous and ferric iron in olivine (Teng et al., 2008; Dauphas et al., 2009a), this could potentially be used to estimate the oxygen fugacity of komatiite magmas during their crystallization. Kinetic isotope effects associated with diffusion-limited growth of spinifex crystals may also be present, in which case Fe and Mg isotopic fractionation could be used as crystal growth speedometers (Dauphas, 2007; Watson and Müller, 2009). In deeper parts of the flow, the expected timescale for cooling would have

been sufficiently long that Fe and Mg could have diffused in and out of olivine (Arndt, 1986), which could have fractionated isotopes (Richter et al., 2008, 2009a,b). Identifying such kinetic isotope fractionation would be important for identifying diffusive processes that may have modified magmatic zoning in olivine, which would in turn provide cooling rate estimates. Large temperature gradients in the flow may have induced vertical migration of elements following Soret diffusion (Bouquain et al., 2009). This process is normally associated with large Mg and Fe isotopic fractionation (Richter et al., 2008, 2009a,b; Huang et al., 2009) and thus isotopic analyses could help us recognize the presence of such effects in komatiite magmas. To summarize, Mg and Fe isotopic compositions could help us understand important processes involved in komatiite petrogenesis.

A complication is that most komatiite samples have experienced extensive alteration and the rocks may not have behaved as closed system for Mg and Fe (Lahaye and Arndt, 1996). Identifying the effects of secondary alteration and distinguishing these effects from those due to magmatic processes is an important element of our study.

## 2. SAMPLES AND METHODS

The petrology and geochemistry of the Alexo flow has been described by Barnes et al. (1983), Arndt (1986), Lahaye and Arndt (1996), and Bouquain et al. (2009) and the broader geological context was given by Naldrett and Mason (1968), Naldrett (1979), and Muir and Comba (1979). Samples of volcanic rocks from the Alexo region have been dated at 2.7 Ga (Corfu, 1993, and references therein). The Alexo komatiites belong to the Al-undepleted group of komatiites (i.e., they have chondritic  $\text{Al}_2\text{O}_3/\text{TiO}_2$  and Gd/Yb ratios; Lahaye et al., 1995; Arndt and Lesher, 2004). Light rare earth element (REE) depletion ( $\text{La}/\text{Sm}_N = 0.47$  and radiogenic initial  $\varepsilon_{\text{Nd}(T)} = +3.8$  indicate that Alexo komatiites formed from a mantle that had experienced long-term depletion (Barnes et al., 1983; Lahaye et al., 1995; Lahaye and Arndt, 1996). Trace and major element compositions are consistent with 50% partial melting of a mantle that was  $\sim 300^\circ\text{C}$  hotter than the modern MORB mantle (Arndt, 2003; Herzberg et al., 2007). The very high temperatures inferred for the Alexo komatiites are consistent with an origin in a plume within a mantle that was hotter than present, which provides a unique constraint on secular cooling of the Earth since the Archean (Richter, 1985; Nisbet et al., 1993). Although all rocks have been subject to low-temperature metamorphism and have been altered by hydrothermal fluids, they are relatively well preserved compared to komatiites from other localities. For instance, up to 80% of cumulus and spinifex olivine has escaped serpentinization (Barnes et al., 1983) and fluid inclusions preserved in these olivine crystals record  $^3\text{He}/^4\text{He}$  ratios up to  $\sim 73$  Ra (after correction for radiogenic  $^4\text{He}$  released by crushing; Richard et al., 1996; Matsumoto et al., 2002). All samples have experienced prehnite-pumpellyite facies metamorphism (Jolly, 1982) and retain most of their original textures. Alteration took several forms (Table 1) including sulfidization, hydration, serpentinization, and rodingitization (i.e., Ca metasomatism associated with

Table 1  
Chemical compositions of komatiites from Alexo.

Sample	Layer	Depth (m)	Alteration	Major elements (wt%), renormalized to 100% volatile-free basis																
				SiO <sub>2</sub>	Al <sub>2</sub> O <sub>3</sub>	Cr <sub>2</sub> O <sub>3</sub>	Fe <sub>2</sub> O <sub>3</sub> *	FeO*	NiO	MnO	MgO	CaO	Na <sub>2</sub> O	K <sub>2</sub> O	TiO <sub>2</sub>	P <sub>2</sub> O <sub>5</sub>	Al/Fe <sup>2+</sup> *	Mn/Fe <sup>2+</sup> *	Mg/Fe <sup>2+</sup>	Fe <sup>3+</sup> /Fe <sup>2+</sup>
M667	X Breccia	1	Hyd!!	45.56	6.67	0.44	0.79	10.19	0.21	0.18	30.71	4.85	0.03	0.03	0.33	n.d.	0.922	0.0181		
M666	Chill margin	2	Hyd, S	45.75	7.05	0.43	0.89	10.08	0.21	0.17	28.12	6.55	0.29	0.10	0.35	n.d.	0.986	0.0172	5.99	0.32
M662	Random	2.2	Hyd, S	45.40	6.36	0.41	0.79	9.73	0.26	0.16	29.86	6.15	0.44	0.10	0.32	n.d.	0.921	0.0168		
M663	Random	3.2	Hyd, S	45.67	6.86	0.43	0.86	10.02	0.24	0.16	28.63	6.25	0.42	0.11	0.34	n.d.	0.964	0.0163	6.66	0.40
M651	Random	3.4	Hyd	45.92	6.56	0.38	0.79	9.55	0.21	0.16	29.47	6.26	0.28	0.08	0.34	n.d.	0.968	0.0171		
M652	X Chevron	4.1	Hyd	45.06	5.66	0.34	0.64	9.25	0.25	0.14	33.04	5.05	0.23	0.06	0.30	n.d.	0.862	0.0155		
M653	X Chevron	5.5	Hyd	45.02	5.35	0.33	0.59	9.10	0.25	0.13	34.02	4.64	0.20	0.06	0.29	n.d.	0.829	0.0146		
M654	X Chevron	6.3	Hyd	44.18	5.04	0.39	0.59	9.64	0.30	0.12	35.00	4.44	0.03	0.01	0.26	n.d.	0.737	0.0127		
M655	Plate	7.1	Rod	44.84	6.77	0.38	0.76	9.04	0.21	0.15	29.18	8.28	0.03	0.01	0.35	n.d.	1.055	0.0170		
M665	Plate	7.8	Hyd	45.17	6.77	0.43	0.87	9.95	0.20	0.16	28.50	7.48	0.07	0.04	0.37	n.d.	0.959	0.0165		
M656	X Plate	8.2	Rod	44.98	7.95	0.46	1.08	10.17	0.16	0.21	23.75	10.67	0.12	0.04	0.41	n.d.	1.102	0.0211		
M668	X Plate	8.7	Hyd	46.48	8.73	0.44	1.13	10.58	0.13	0.16	23.85	7.92	0.09	0.04	0.45	n.d.	1.162	0.0155		
M668	Plate (olivine-ol)	8.7	Hyd	46.52	7.24	n.d.	0.85	9.99	n.d.	0.17	29.07	5.74	0.05	0.00	0.37	n.d.	1.022	0.0175		
AX105	X Plate	8.7	Hyd	46.80	7.36	n.d.	0.94	9.56	n.d.	0.17	28.24	6.42	0.09	0.00	0.37	0.05	1.085	0.0183	6.07	0.25
AX107	X Plate	8.7	Hyd	46.57	8.14	n.d.	1.08	10.18	n.d.	0.21	25.81	7.27	0.19	0.08	0.43	0.05	1.127	0.0208	4.69	0.14
M657	Plate	9.5	Rod	43.73	9.51	0.50	1.34	11.00	0.09	0.18	20.14	12.96	0.03	0.01	0.51	n.d.	1.219	0.0168	3.50	0.17
M658	X Plate	10.2	Rod	43.83	6.06	0.43	0.80	10.00	0.24	0.18	30.10	7.98	0.04	0.01	0.32	n.d.	0.854	0.0184		
M710	X B1	11.5	Hyd	43.98	6.52	n.d.	0.90	9.70	n.d.	0.20	29.99	8.34	0.00	0.00	0.34	0.05	0.948	0.0204	8.85	0.74
M661	X Cumulate	13	Hyd!	44.03	3.22	0.32	0.26	8.02	0.38	0.12	42.42	1.01	0.01	0.01	0.19	n.d.	0.567	0.0153	20.36	1.30
M713	X Cumulate	14.5	Hyd-	44.78	3.81	0.29	0.20	6.95	0.33	0.14	43.07	0.20	n.d.	n.d.	0.21	0.01	0.773	0.0205	20.07	1.15
M712	X Cumulate	15.5	Hyd-	44.64	3.72	0.29	0.32	7.67	0.32	0.16	39.82	2.82	n.d.	0.01	0.21	0.02	0.683	0.0212	17.06	1.05
M712	Cumulate (olivine separate)	15.5		40.79	0.08	0.27		7.58	0.42	0.11	50.46	0.23	0.01	0.00	0.04	n.d.	0.016	0.0146		
Initial liquid				45.61	6.76	0.42	0.85	9.94	0.24	0.16	28.87	6.32	0.39	0.10	0.34	n.d.	0.957	0.0168		
Average olivine				40.88	0.07	0.21		7.97	0.41	0.12	50.13	0.21					0.012	0.0159		

Bulk major and minor element concentrations are from Arndt (1986), Lahaye and Arndt (1996), and new data reported here for M668-ol, AX105, AX107, M710, and M712 olivine. The Mg/Fe<sup>2+</sup> and Fe<sup>3+</sup>/Fe<sup>2+</sup> ratios given in the last two columns were calculated from actual MgO, FeO and Fe<sub>2</sub>O<sub>3</sub> concentration measurements at Service d'Analyse des Roches et des Mineraux, Nancy-France (total Fe<sub>2</sub>O<sub>3</sub> by atomic absorption and FeO by volumetric titration). The initial liquid composition is the average of M666, M662, and M663 (Lahaye and Arndt, 1996). The average olivine composition is from Sobolev et al. (2007). FeO\* and Fe<sub>2</sub>O<sub>3</sub>\* concentrations were calculated from bulk Fe<sub>2</sub>O<sub>3</sub> by assuming Fe<sup>3+</sup>/Fe<sub>tot</sub> = 0.07 at 29.1 wt% MgO (initial liquid), Fe<sup>3+</sup>/Fe<sub>tot</sub> = 0 at 51 wt% MgO (olivine), and using linear interpolation/extrapolation. Al/Fe<sup>2+</sup> and Mn/Fe<sup>2+</sup> ratios were calculated using FeO\*. The samples marked with an X do not follow a trend of magmatic differentiation in Al/Fe<sup>2+</sup> vs Mn/Fe<sup>2+</sup> diagram (Fig. 6). Hyd, S, and Rod stand for hydration, sulfide-addition, and rodingitization, respectively. Hyd-, !, !! stand for low, high, and very high hydration.

serpentinization reactions; Schandl et al., 1989). This alteration affected to various extents the chemical compositions of the lavas (Lahaye and Arndt, 1996), but a combination of petrographic and geochemical data usually allows the effects of alteration to be monitored. Komatiites from Alexo show clear evidence for olivine-controlled magmatic differentiation (Arndt, 1986; Lahaye and Arndt, 1996) and comparison between predicted olivine-control lines with actual data allows one to quantify net loss or gain of a particular element during alteration (Lahaye and Arndt, 1996). Even elements like the REE, which are relatively insoluble in usual metamorphic and hydrothermal fluids, show evidence of metasomatic alteration in certain samples (Lahaye et al., 1995).

The 17-m thick lava flow can be subdivided into several units from top to bottom (Fig. 1). At the top, a flow breccia is underlain by a chilled margin. Samples from these two units are thought to be representative of the lava before differentiation. The average composition of 3 such samples (recalculated on a water-free basis) is given in Table 1 (also, see Lahaye and Arndt, 1996). The initial lava had a MgO of 29.1 wt%, corresponding to an anhydrous olivine liquidus temperature at 1 atmosphere of  $\sim 1580$  °C (Beattie, 1993). The most forsteritic olivines have an Mg#  $[\text{Mg}/(\text{Mg} + \text{Fe})_{\text{at}}]$  of 94.1, consistent with a starting MgO content of 29.1 wt% (Arndt, 1986). Below the chill margin are random spinifex, chevron spinifex, and plate spinifex samples.

The texture and crystallization sequence of this spinifex unit have been the focus of much discussion. In particular, phase relationships (Kinzler and Grove, 1985) would predict that olivine should crystallize first and that augite should crystallize before pigeonite while the opposite is observed in the lower part of the spinifex zone (Bouquain et al., 2009). Bouquain et al. suggested that Soret differentiation of the liquid trapped in the crystal mush could explain the early crystallization of pigeonite. Crystallization

in temperature gradients produces the spinifex texture (Faure et al., 2006).

Below the spinifex layer is the B1 horizon, which contains equant to elongate hopper olivine crystals showing a preferred orientation parallel to the top of the flow (Pyke et al., 1973; Arndt, 1986). Further down is an olivine cumulate containing relatively large ( $\sim 0.5$  mm) olivine grains. Studying a profile within a flow can help understand the relationships between the different units, but one should bear in mind that some lateral magma transfer could have taken place (Barnes et al., 1983; Arndt, 1986).

The nature and alteration type of all 22 samples analyzed in this study are presented in Table 1 and Fig. 1. They comprise 1 flow top breccia (M667), 1 chill margin (M666), 3 random spinifex (M662, M663, M651), 3 chevron spinifex (M652, M653, M654), 8 plate spinifex (M655, M665, M656, M668, AX105, AX107, M657, M658), 1 B1 unit (M710), and 3 cumulate samples (M661, M713, M712).

Sample M668-ol is the olivine-rich portion of M668 that was obtained after sawing out the non-olivine rich parts between spinifex crystals. Sample M712 olivine is an olivine separate from M712, which was obtained by crushing the sample and concentrating olivine grains using heavy liquids and Frantz magnetic separation.

Iron isotopic analyses were carried out following the method presented by Dauphas et al. (2004, 2009b). Most samples were ground in alumina or agate mills at the Max-Planck-Institute in Mainz; others were ground in an agate mortar in Chicago. Approximately 10–20 mg aliquots from several grams of homogenized powder were digested in acid. Iron was then separated from matrix elements and isobaric interferences using AG1-X8 anion exchange resin in hydrochloric acid medium. The chemical separation procedure was repeated twice. After purification, Fe isotopes were analyzed using a *Thermo Scientific Neptune MC-ICPMS* (Multi-Collector Inductively Coupled Plasma Mass Spectrometer) at the Origins Laboratory of the

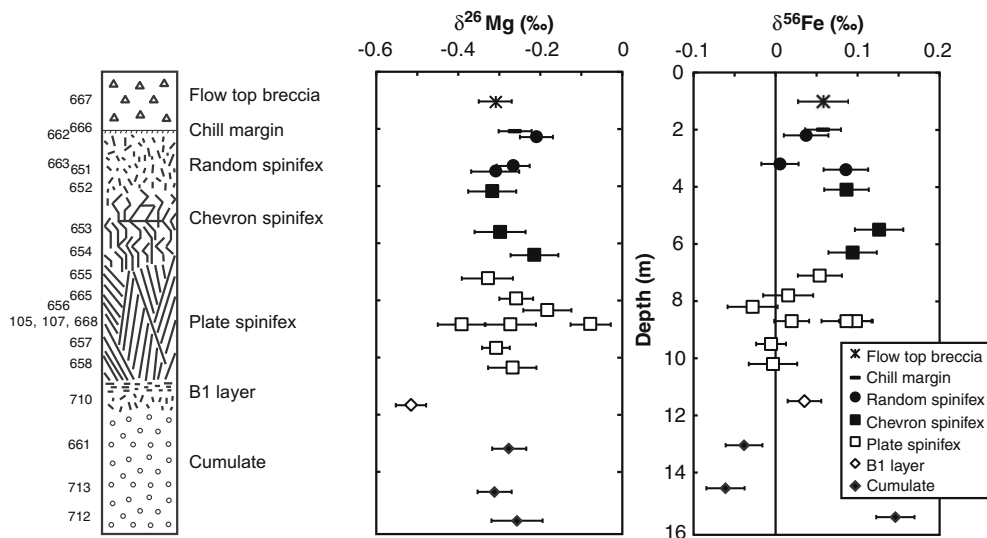


Fig. 1. Depth profiles of  $\delta^{56}\text{Fe}$  and  $\delta^{26}\text{Mg}$  values in Alexo flow (bulk data from Table 2). Arndt (1986), Lahaye and Arndt (1996), and Bouquain et al. (2009) provided details on the petrography and chemistry of the samples analyzed in this study.

University of Chicago. Instrumental mass fractionation was corrected for using sample-standard bracketing and Fe isotope variations are reported in permil deviation relative to the composition of reference material IRMM-014, which has a composition very similar to chondrites:  $\delta^i\text{Fe} = [(^i\text{Fe}/^{54}\text{Fe})_{\text{sample}} / (^i\text{Fe}/^{54}\text{Fe})_{\text{IRMM-014}} - 1] \times 1000$ , where  $i = 56$  or  $57$ . Iron isotope variations in igneous rocks span a narrow range of  $\sim 0.3\text{‰}$ . Dauphas et al. (2009b) demonstrated that the isotopic analyses were accurate within the quoted uncertainty of approximately  $\pm 0.03\text{‰}$ . Here and throughout the text, uncertainties are quoted at the 95% confidence level. The chemical compositions of all samples are compiled in Table 1 (also, see Arndt, 1986; Lahaye and Arndt, 1996).

Magnesium isotopic analyses were performed at the Isotope Laboratory of the University of Arkansas, Fayetteville following the method described by Yang et al. (2009). All chemical procedures were carried out in a clean laboratory environment. Approximately 1 mg aliquots from several grams of homogenized powder were dissolved in Savillex screw-top beakers in mixtures of concentrated HF–HNO<sub>3</sub> ( $\sim 3:1$ ), followed by HNO<sub>3</sub>–HCl ( $\sim 3:1$ ) and the residues were finally dissolved in 1 N HNO<sub>3</sub> in preparation for chromatographic separation. Separation of Mg was achieved by cation exchange chromatography with Bio-Rad 200–400 mesh AG50W-X8 pre-cleaned resin in 1 N HNO<sub>3</sub> following an established procedure described by Teng et al. (2007) and Yang et al. (2009). Samples containing  $\sim 50$   $\mu\text{g}$  of Mg were loaded onto the resin and Mg was eluted with 1 N HNO<sub>3</sub>. This procedure was repeated in order to obtain pure Mg solutions for mass spectrometry. Magnesium isotopic compositions were analyzed by the standard bracketing method using a *Nu Plasma* MC-ICPMS at the University of Arkansas. Magnesium isotope variations are reported in permil deviation relative to the composition of reference material DSM-3, a solution made from pure Mg metal (Galy et al., 2003):  $\delta^i\text{Mg} = [(^i\text{Mg}/^{24}\text{Mg})_{\text{sample}} / (^i\text{Mg}/^{24}\text{Mg})_{\text{DSM-3}} - 1] \times 1000$ , where  $i = 25$  or  $26$ . Multiple analyses of synthetic solution, rock and mineral standards over 1 year demonstrate that accurate measurements at a precision better than  $0.1\text{‰}$  can be routinely achieved.

### 3. RESULTS

Except for 2 outliers ( $\delta^{26}\text{Mg} = -0.073 \pm 0.049\text{‰}$  for the coarse olivine spinifex lava AX105 and  $\delta^{26}\text{Mg} = -0.514 \pm 0.036\text{‰}$  for M710 from the B1 layer), the Mg isotopic compositions of samples from the Alexo flow are homogeneous (Table 2 and Fig. 1). The  $\delta^{26}\text{Mg}$  values of the two outliers were replicated (from chemical separation to isotopic analysis, starting from the same solution of digested powder) and the results are reproducible ( $\delta^{26}\text{Mg} = -0.081 \pm 0.062\text{‰}$  vs.  $-0.060 \pm 0.080\text{‰}$  for AX105;  $\delta^{26}\text{Mg} = -0.517 \pm 0.041\text{‰}$  vs.  $-0.500 \pm 0.080\text{‰}$  for M710). The average  $\delta^{25}\text{Mg}$  and  $\delta^{26}\text{Mg}$  values of the remaining 19 samples are  $-0.140 \pm 0.011\text{‰}$  and  $-0.275 \pm 0.022\text{‰}$ , respectively. These are, to our knowledge, the first measurements of the Mg isotopic composition of komatiitic magmas. The value we obtained is indistinguishable from the average composition of terrestrial mantle peridotites,

which was taken by Handler et al. (2009), Yang et al. (2009) and Teng et al. (2010) to represent the Mg isotopic composition of the BSE. It is also indistinguishable from Mg isotopic measurements of basalts reported by several groups (e.g., Young and Galy, 2004; Baker et al., 2005; Teng et al., 2007, 2010; Tipper et al., 2008). The olivine-rich portion of komatiite M668 has a slightly heavier Mg isotopic composition than the bulk sample ( $\delta^{26}\text{Mg} = -0.236 \pm 0.058\text{‰}$  vs.  $-0.389 \pm 0.058\text{‰}$ ).

Bulk komatiite samples from Alexo have Fe isotopic compositions that range from  $-0.06\text{‰}$  to  $+0.15\text{‰}$  (Table 2 and Fig. 1). The  $0.2\text{‰}$  dispersion that is observed is significantly higher than the analytical uncertainty and must be real. Many samples were replicated (from dissolution to MC-ICPMS measurement) and all these analyses yield reproducible iron isotopic compositions (i.e.,  $\delta^{56}\text{Fe} = +0.062, +0.051\text{‰}$  for M666;  $+0.006, +0.004$  for M663;  $+0.097, +0.099$  for AX105;  $+0.034, +0.002$  for AX107;  $+0.008, -0.017, -0.017, -0.007$  for M657;  $+0.023, +0.052$  for M710;  $-0.048, -0.024$  for M661;  $-0.063, -0.059$  for M713;  $+0.145, +0.148$  for M712). A potential concern is the fact that some powders were prepared in Chicago from small hand specimens and that these might not be representative of the bulk samples analyzed previously by Arndt (1986) and Lahaye and Arndt (1996) if significant heterogeneity was present at the bulk sample scale. This was addressed by measuring the Fe isotopic composition of M657 from a large batch of homogenized powder used in previous publications (Arndt, 1986; Lahaye and Arndt, 1996). There is no difference between that value ( $\delta^{56}\text{Fe} = +0.008 \pm 0.031\text{‰}$ ) and the two values measured from powder prepared in Chicago ( $\delta^{56}\text{Fe} = -0.017 \pm 0.029\text{‰}$  and  $-0.007 \pm 0.037\text{‰}$ ). Major element compositions of some powders prepared in Chicago were also analyzed at Service d'Analyse des Roches et des Minéraux in Nancy, France and very good agreement was found with previously published data.

The widest dispersion is found in three cumulate samples; two have negative values ( $\delta^{56}\text{Fe} = -0.04\text{‰}$  and  $-0.06\text{‰}$ , for M661 and M713, respectively) and the third has a positive value ( $\delta^{56}\text{Fe} = +0.15\text{‰}$  for M712). There is no relationship between the isotopic compositions and the localities of these samples – M661 comes from the eastern outcrop and M712 and M713 from the western outcrop – nor with their composition and degree of alteration – M661 and M713 are completely serpentinized whereas M712 retains a large proportion of fresh olivine.

To our knowledge, the Fe isotopic compositions of only 2 bulk komatiites were measured at high precision prior to the present work. Poitrasson et al. (2004) reported a  $\delta^{56}\text{Fe}$  value of  $+0.038 \pm 0.016\text{‰}$  for WITS-1, a 3.5 Ga komatiite from Barberton, South Africa. Weyer and Ionov (2007) measured a value of  $+0.071 \pm 0.022$  for KAL-1, a komatiite from Alexo, Ontario. Sample M666 was taken at the same location as KAL-1 and has identical Fe isotopic composition within uncertainties ( $+0.058 \pm 0.022\text{‰}$ ).

The  $\text{Fe}^{3+}/\text{Fe}^{2+}$  ratio was analyzed at SARM in a subset of samples (M666, M663, AX105, AX107, M657, M710, M661, M713, M712, Table 1) and was found to be variable and elevated (from 0.24 for plate spinifex AX-107 to 1.40

Table 2

Mg and Fe isotopic compositions of komatiites from Alexo.

Sample	Layer (mineral)	Depth (m)	Alteration	Individual analyzes				Averages of replicate analyzes			
				$\delta^{25}\text{Mg}$ (‰)	$\delta^{26}\text{Mg}$ (‰)	$\delta^{56}\text{Fe}$ (‰)	$\delta^{57}\text{Fe}$ (‰)	$\delta^{25}\text{Mg}$ (‰)	$\delta^{26}\text{Mg}$ (‰)	$\delta^{56}\text{Fe}$ (‰)	$\delta^{57}\text{Fe}$ (‰)
M667	X Breccia	1	Hyd!!	$-0.150 \pm 0.040$	$-0.305 \pm 0.041$	$0.058 \pm 0.029$	$0.061 \pm 0.032$	$-0.150 \pm 0.040$	$-0.305 \pm 0.041$	$0.058 \pm 0.029$	$0.061 \pm 0.032$
M666	Chill margin	2	Hyd, S	$-0.136 \pm 0.040$	$-0.260 \pm 0.041$	$0.062 \pm 0.027$	$0.076 \pm 0.040$	$-0.136 \pm 0.040$	$-0.260 \pm 0.041$	$0.058 \pm 0.022$	$0.082 \pm 0.030$
						$0.051 \pm 0.037$	$0.090 \pm 0.045$				
M662	Random	2.2	Hyd, S	$-0.122 \pm 0.040$	$-0.206 \pm 0.041$	$0.037 \pm 0.027$	$0.056 \pm 0.026$	$-0.122 \pm 0.040$	$-0.206 \pm 0.041$	$0.037 \pm 0.027$	$0.056 \pm 0.026$
M663	Random	3.2	Hyd, S	$-0.123 \pm 0.040$	$-0.263 \pm 0.041$	$0.006 \pm 0.029$	$0.006 \pm 0.043$	$-0.123 \pm 0.040$	$-0.263 \pm 0.041$	$0.005 \pm 0.023$	$-0.001 \pm 0.031$
						$0.004 \pm 0.037$	$-0.008 \pm 0.045$				
M651	Random	3.4	Hyd	$-0.155 \pm 0.049$	$-0.307 \pm 0.058$	$0.086 \pm 0.027$	$0.123 \pm 0.026$	$-0.155 \pm 0.049$	$-0.307 \pm 0.058$	$0.086 \pm 0.027$	$0.123 \pm 0.026$
M652	X Chevron	4.1	Hyd	$-0.169 \pm 0.049$	$-0.314 \pm 0.058$	$0.086 \pm 0.027$	$0.123 \pm 0.026$	$-0.169 \pm 0.049$	$-0.314 \pm 0.058$	$0.086 \pm 0.027$	$0.123 \pm 0.026$
M653	X Chevron	5.5	Hyd	$-0.159 \pm 0.040$	$-0.295 \pm 0.062$	$0.126 \pm 0.029$	$0.164 \pm 0.032$	$-0.159 \pm 0.040$	$-0.295 \pm 0.062$	$0.126 \pm 0.029$	$0.164 \pm 0.032$
M654	X Chevron	6.3	Hyd	$-0.110 \pm 0.049$	$-0.211 \pm 0.058$	$0.094 \pm 0.029$	$0.137 \pm 0.032$	$-0.110 \pm 0.049$	$-0.211 \pm 0.058$	$0.094 \pm 0.029$	$0.137 \pm 0.032$
M655	Plate	7.1	Rod	$-0.151 \pm 0.040$	$-0.326 \pm 0.062$	$0.053 \pm 0.027$	$0.055 \pm 0.026$	$-0.151 \pm 0.040$	$-0.326 \pm 0.062$	$0.053 \pm 0.027$	$0.055 \pm 0.026$
M665	Plate	7.8	Hyd	$-0.118 \pm 0.040$	$-0.256 \pm 0.041$	$0.015 \pm 0.031$	$0.027 \pm 0.036$	$-0.118 \pm 0.040$	$-0.256 \pm 0.041$	$0.015 \pm 0.031$	$0.027 \pm 0.036$
M656	X Plate	8.2	Rod	$-0.097 \pm 0.049$	$-0.180 \pm 0.058$	$-0.028 \pm 0.031$	$-0.021 \pm 0.036$	$-0.097 \pm 0.049$	$-0.180 \pm 0.058$	$-0.028 \pm 0.031$	$-0.021 \pm 0.036$
M668	X Plate	8.7	Hyd	$-0.204 \pm 0.049$	$-0.389 \pm 0.058$	$0.086 \pm 0.031$	$0.161 \pm 0.036$	$-0.204 \pm 0.049$	$-0.389 \pm 0.058$	$0.086 \pm 0.031$	$0.161 \pm 0.036$
M668-ol	Plate (olivine-rich)	8.7	Hyd	$-0.113 \pm 0.049$	$-0.236 \pm 0.058$	$0.028 \pm 0.039$	$0.031 \pm 0.058$	$-0.113 \pm 0.049$	$-0.236 \pm 0.058$	$0.028 \pm 0.039$	$0.031 \pm 0.058$
AX105	X Plate	8.7	Hyd	$-0.024 \pm 0.040$	$-0.081 \pm 0.062$	$0.097 \pm 0.027$	$0.164 \pm 0.040$	$-0.027 \pm 0.031$	$-0.073 \pm 0.049$	$0.098 \pm 0.021$	$0.158 \pm 0.029$
				$-0.030 \pm 0.050$	$-0.060 \pm 0.080$	$0.099 \pm 0.031$	$0.152 \pm 0.042$				
AX107	X Plate	8.7	Hyd	$-0.138 \pm 0.040$	$-0.269 \pm 0.062$	$0.034 \pm 0.029$	$0.057 \pm 0.043$	$-0.138 \pm 0.040$	$-0.269 \pm 0.062$	$0.020 \pm 0.021$	$0.026 \pm 0.029$
						$0.002 \pm 0.031$	$0.000 \pm 0.039$				
M657	Plate	9.5	Rod	$-0.136 \pm 0.049$	$-0.304 \pm 0.058$	$0.008 \pm 0.031$	$0.006 \pm 0.036$	$-0.139 \pm 0.031$	$-0.305 \pm 0.033$	$-0.006 \pm 0.018$	$0.000 \pm 0.024$
				$-0.141 \pm 0.040$	$-0.306 \pm 0.041$	$-0.017 \pm 0.029$	$-0.007 \pm 0.043$				
						$-0.007 \pm 0.037$	$0.000 \pm 0.049$				
M658	X Plate	10.2	Rod	$-0.144 \pm 0.049$	$-0.265 \pm 0.058$	$-0.003 \pm 0.029$	$-0.005 \pm 0.032$	$-0.144 \pm 0.049$	$-0.265 \pm 0.058$	$-0.003 \pm 0.029$	$-0.005 \pm 0.032$
M710	X B1	11.5	Hyd	$-0.251 \pm 0.040$	$-0.517 \pm 0.041$	$0.023 \pm 0.027$	$0.039 \pm 0.040$	$-0.254 \pm 0.031$	$-0.514 \pm 0.036$	$0.035 \pm 0.021$	$0.058 \pm 0.029$
				$-0.260 \pm 0.050$	$-0.500 \pm 0.080$	$0.052 \pm 0.031$	$0.078 \pm 0.042$				
M661	X Cumulate	13	Hyd!	$-0.146 \pm 0.040$	$-0.274 \pm 0.041$	$-0.048 \pm 0.027$	$-0.059 \pm 0.040$	$-0.146 \pm 0.040$	$-0.274 \pm 0.041$	$-0.039 \pm 0.022$	$-0.048 \pm 0.031$
						$-0.024 \pm 0.037$	$-0.033 \pm 0.049$				
M713	X Cumulate	14.5	Hyd-	$-0.149 \pm 0.040$	$-0.309 \pm 0.041$	$-0.063 \pm 0.030$	$-0.084 \pm 0.045$	$-0.149 \pm 0.040$	$-0.309 \pm 0.041$	$-0.061 \pm 0.023$	$-0.092 \pm 0.032$
						$-0.059 \pm 0.037$	$-0.100 \pm 0.045$				
M712	X Cumulate	15.5	Hyd-	$-0.133 \pm 0.040$	$-0.253 \pm 0.062$	$0.145 \pm 0.030$	$0.197 \pm 0.045$	$-0.133 \pm 0.040$	$-0.253 \pm 0.062$	$0.146 \pm 0.023$	$0.213 \pm 0.032$
						$0.148 \pm 0.037$	$0.227 \pm 0.045$				
M712 olivine	Cumulate (olivine separate)	15.5		$-0.109 \pm 0.048$	$-0.234 \pm 0.087$	$-0.323 \pm 0.060$	$-0.560 \pm 0.072$	$-0.109 \pm 0.048$	$-0.234 \pm 0.087$	$-0.316 \pm 0.034$	$-0.502 \pm 0.047$
						$-0.313 \pm 0.041$	$-0.457 \pm 0.063$				

Uncertainties are 95% confidence intervals.  $\delta^i\text{Fe} = [(^i\text{Fe}/^{54}\text{Fe})_{\text{sample}}/(^i\text{Fe}/^{54}\text{Fe})_{\text{IRMM-014}} - 1] \times 10^3$ ,  $\delta^i\text{Mg} = [(^i\text{Mg}/^{24}\text{Mg})_{\text{sample}}/(^i\text{Mg}/^{24}\text{Mg})_{\text{DSM-3}} - 1] \times 10^3$ .

The samples marked with an X do not follow the trend of magmatic differentiation in Al/Fe<sup>2+</sup>\* vs Mn/Fe<sup>2+</sup>\* diagram (Fig. 6) and may have been affected by secondary Fe mobilization. Hyd, S, and Rod stand for hydration, sulfide-addition, and rodingitization, respectively. Hyd-, !, !! stand for low, high, and very high hydration.

for highly hydrated cumulate M661). The  $\text{Fe}^{3+}/\text{Fe}^{2+}$  ratio correlates positively with MgO content (Fig. 2), reflecting the sensitivity of olivine-rich samples to serpentinization and Fe oxidation. Assuming that Mg is bound to olivine and that olivine is entirely serpentinized into magnetite and other phases, one would expect a correlation between  $\text{Fe}^{3+}/\text{Fe}^{2+}$  and  $\text{Mg}^{2+}/\text{Fe}^{2+}$  with a slope approximately equal to  $2/3 \times (\text{Fe}/\text{Mg})_{\text{olivine}}$ . The  $2/3$  factor arises from the fact that during formation of magnetite, only 2 atoms of  $\text{Fe}^{2+}$  out of 3 are converted into  $\text{Fe}^{3+}$ . For a Fe/Mg ratio in olivine of 8/92, the predicted slope is  $\sim 0.06$ . The measured slope of  $0.065 \pm 0.015$  is identical within uncertainty to that value. This is analogous to correlations between  $\text{H}_2\text{O}$  and MgO content found in most komatiite suites, which reflect the fact that olivine alters to  $\text{H}_2\text{O}$ -rich minerals whereas pyroxene and plagioclase alter to  $\text{H}_2\text{O}$ -poor minerals (Smith and Erlank, 1982; Nisbet et al., 1993).

For the purpose of understanding magmatic differentiation, it is important to distinguish ferrous from ferric iron. Because directly measured  $\text{Fe}^{3+}/\text{Fe}^{2+}$  ratios cannot be used for this purpose, pre-alteration  $\text{FeO}^*$  and  $\text{Fe}_2\text{O}_3^*$  (marked with \*, Table 1) were calculated from bulk  $\text{Fe}_2\text{O}_3$  by assuming  $\text{Fe}^{3+}/\text{Fe}_{\text{total}} = 0.07$  at 29.1 wt% MgO (initial liquid),  $\text{Fe}^{3+}/\text{Fe}_{\text{total}} = 0$  at 51 wt% MgO (pure olivine), and using simple linear interpolation/extrapolation. The initial liquid  $\text{Fe}^{3+}/\text{Fe}^{2+}$  ratio corresponds to 50% partial melting of a source with  $\text{Fe}^{3+}/\text{Fe}^{2+} = 0.037$  using liquid/solid partition coefficients for  $\text{Fe}^{2+}$  and  $\text{Fe}^{3+}$  of 1 and 10, respectively (Canil et al., 1994).

While there are correlations between  $\text{FeO}^*$  and MgO content with  $\text{Al}_2\text{O}_3$  that reflect magmatic differentiation (Fig. 3), there is no clear correlation between  $\delta^{56}\text{Fe}$  and MgO (Fig. 4). There is a crude positive correlation for samples with MgO contents between 24 and 34 wt% but this is opposite to the magmatic differentiation trend observed in Kilauea Iki lava lake (Teng et al., 2008). The three samples that were used by Lahaye and Arndt to define the initial composition of the liquid (M666, M662, and M663) have similar, yet resolvable  $\delta^{56}\text{Fe}$  values of  $+0.058 \pm 0.022$ ,  $+0.037 \pm 0.027$ , and  $+0.005 \pm 0.023\%$ .

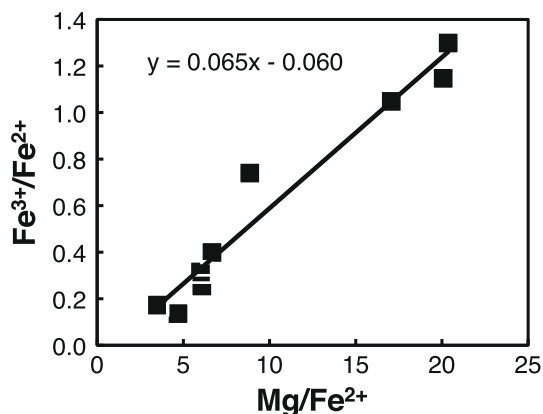


Fig. 2. Correlation between iron oxidation state and magnesium content. The positive correlation between  $\text{Fe}^{3+}/\text{Fe}^{2+}$  and  $\text{Mg}/\text{Fe}^{2+}$  reflects the fact that Mg-rich samples are rich in olivine, which is prone to serpentinization, a process that converts  $\text{Fe}^{2+}$  into  $\text{Fe}^{3+}$  (data from Table 1).

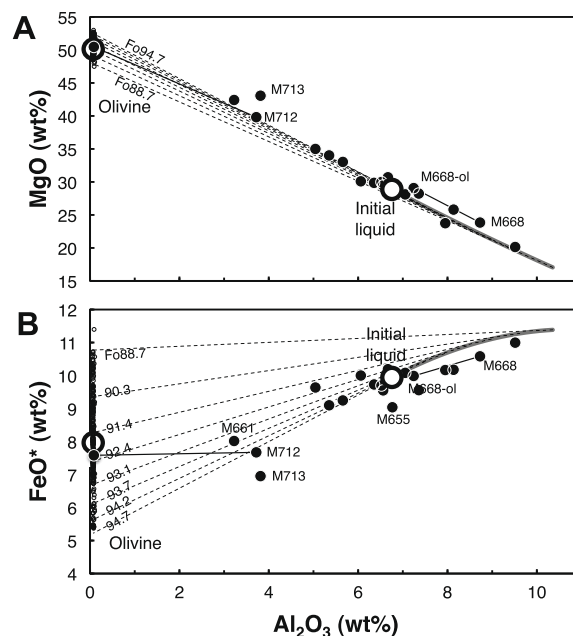


Fig. 3. Magmatic differentiation trends for Mg (A) and Fe (B). Olivine data on the left are from Sobolev et al. (2007). Bulk rock data are from Table 1, and references therein.  $\text{FeO}^*$  was calculated from total iron by assuming  $\text{Fe}^{3+}/(\text{Fe}^{3+} + \text{Fe}^{2+}) = 0.07$  at 29.1 wt% MgO (initial liquid),  $\text{Fe}^{3+}/(\text{Fe}^{3+} + \text{Fe}^{2+}) = 0$  at 51 wt% MgO (olivine), and using linear interpolation/extrapolation. The grey line represents evolution of the liquid by fractional crystallization of olivine. Olivine composition in equilibrium with liquid was calculated using the parameterization for the exchange coefficient  $(\text{Fe}^{2+}/\text{Mg})_{\text{ol}}/(\text{Fe}^{2+}/\text{Mg})_{\text{Liq}}$  of Toplis (2005). The dashed lines connect predicted olivine and liquid compositions. The thin solid lines connect the bulk and olivine-rich portions of samples M668 and M712. The Fo content of olivine is the ratio  $\text{Mg}/(\text{Fe} + \text{Mg})$ . See text for discussion.

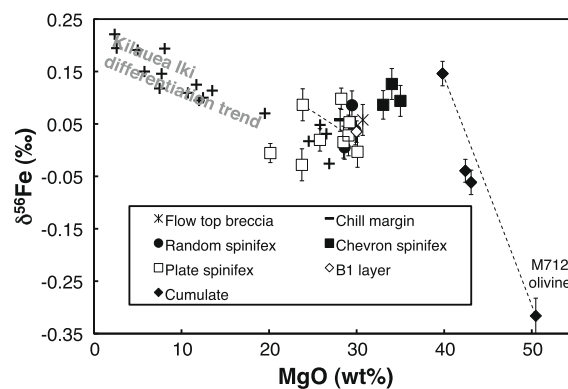


Fig. 4. Magmatic differentiation and Fe isotopic fractionation in Alexo komatiite flow. The MgO content of the primary liquid is  $\sim 29.1$  wt% (average of M666, M662, and M663, Lahaye and Arndt, 1996). The magmatic differentiation trend observed at Kilauea Iki lava lake is shown for comparison (Teng et al., 2008). The thin dashed lines correspond to mixing between the bulk and olivine-rich portions of M668 and M712.

The olivine separate from cumulate sample M712 gave  $\delta^{26}\text{Mg} = -0.234 \pm 0.087\%$  and  $\delta^{56}\text{Fe} = -0.316 \pm 0.034\%$ , a Fe isotopic composition that is much lighter than that of

the whole rocks. The olivine-rich portion of plate spinifex sample M668 is also slightly isotopically lighter ( $\delta^{56}\text{Fe} = +0.028 \pm 0.039\text{‰}$ ) than the bulk sample ( $\delta^{56}\text{Fe} = +0.086 \pm 0.031\text{‰}$ ). In chemical composition diagrams (Fig. 3), the two samples (M668 and M668-ol) define segments that are parallel to the trend of magmatic differentiation. In a diagram  $\delta^{56}\text{Fe}$  vs MgO (Fig. 4), the two samples are parallel to the trend of magmatic differentiation observed in Kilauea Iki lava lake (Teng et al., 2008). Assuming that M668-ol is a mixture between bulk M668 and an olivine end-member at 51 wt.% MgO, one can calculate the iron isotopic composition of olivine. This is not a simple linear extrapolation as the bulk sample and olivine have different Fe concentrations so that mixing in  $\delta^{56}\text{Fe}$  vs. MgO diagram should show some curvature,

$$\delta_{\text{olivine}} = \delta_{\text{M668-ol}} + (\delta_{\text{M668}} - \delta_{\text{M668-ol}}) \times \frac{[\text{Fe}]_{\text{M668}}}{[\text{Fe}]_{\text{olivine}}} \left( \frac{[\text{Mg}]_{\text{M668-ol}} - [\text{Mg}]_{\text{olivine}}}{[\text{Mg}]_{\text{M668-ol}} - [\text{Mg}]_{\text{M668}}} \right)$$

Using appropriate compositions, one estimates  $\delta^{56}\text{Fe}$  of olivine in M668 to be  $-0.34 \pm 0.35\text{‰}$  (Fig. 4), a value identical within error with that of olivine separated from sample M712.

As part of a study of komatiite-hosted Fe–Ni sulfide deposits, Bekker et al. (2009) analyzed 5 olivine separates from komatiites from the Agnew–Wiluna greenstone belt, Western Australia. The  $\delta^{56}\text{Fe}$  values were all lower than MORB and close to chondritic (i.e.,  $-0.05\text{‰}$ ,  $-0.02\text{‰}$ ,  $-0.04\text{‰}$ ,  $-0.02\text{‰}$ , and  $+0.02\text{‰}$ ).

## 4. DISCUSSION

### 4.1. Isotopic effects of alteration

Komatiites from Alexo are relatively well preserved compared to samples from other localities. For example, volcanic textures (e.g., breccia, spinifex, cumulate) are essentially unaltered and primary magmatic phases (e.g., olivine, pyroxene, chromite, melt inclusions) are partially retained. However, it is well documented that alteration (e.g., serpentinization, rodingitization, and sulfide addition) can mobilize even the most fluid immobile elements like high field strength elements and REE (Lahaye et al., 1995; Lahaye and Arndt, 1996). In that respect, studying samples from a single flow is particularly powerful as one can distinguish chemical variations due to magmatic differentiation from those that are due to secondary alteration. At Alexo, the main control on the evolution of the flow is olivine crystallization. In a plot of  $\text{Cr}_2\text{O}_3$  vs.  $\text{Al}_2\text{O}_3$ , a positive correlation is found, which is consistent with fractional crystallization of olivine (Fig. 5), indicating that chromite did not play an important role in the chemical evolution of the flow (Arndt, 1986). Similarly, substantial fractionation of an immiscible sulfide liquid can be ruled out on the basis of the behavior of platinum group elements (e.g., Pd and Pt) during differentiation (Puchtel et al., 2004). To assess element mobility, one can therefore compare measured chemical compositions with predicted liquid lines of descent and cumulate compositions for fractional

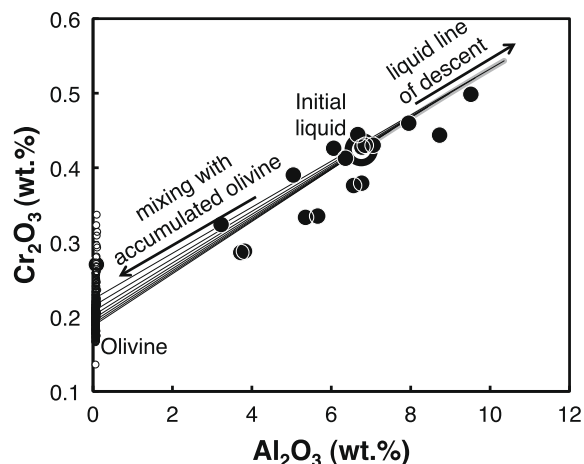


Fig. 5. Magmatic evolution of  $\text{Cr}_2\text{O}_3$ . The fact that most samples plot near the olivine control lines indicates that chromite fractionation did not affect the composition of the flow.

crystallization of olivine. Assuming that  $\text{Al}_2\text{O}_3$  was immobile, Lahaye and Arndt (1996) concluded that most samples did not experience significant gain or loss of Mg and Fe ( $\pm 5\%$  relative), the exceptions being a completely altered sample of flow top breccia (M667) and two completely serpentinized olivine cumulates (M661 and M713). These samples plot slightly above the magmatic trends in Fig. 3 and sample M713 has an unusually low FeO content.

Alteration of oceanic crust is known to induce iron isotopic fractionation. Rouxel et al. (2003) found a negative correlation between  $\delta^{56}\text{Fe}$  and Fe/Ti ratios that they interpreted to reflect removal of a fluid containing isotopically light Fe. Similar fractionation was found during pedogenesis in Hawaii (Thompson et al., 2007). These observations are consistent with laboratory experiments, which show that Fe released by mineral dissolution tends to be enriched in the light isotopes (Beard et al., 2003; Brantley et al., 2004; Icopini et al., 2004; Wiederhold et al., 2006). In detail, the magnitude of the fractionation depends on the presence and nature of ligands in the fluid, the chemical pathway (proton-promoted, ligand-controlled, and reductive dissolution), and bacterial activity. In light of these studies, one must scrutinize whether alteration could have affected the Fe isotopic compositions of the komatiites measured in this study.

The average of samples M666, M662, and M663 was used as the starting composition to calculate trends of magmatic differentiation.  $\text{Fe}^{3+}/\text{Fe}^{2+}$  ratios measured in these samples reflect oxidative alteration (Fig. 2). For that reason,  $\text{FeO}^*$  calculated from bulk  $\text{FeO} + \text{Fe}_2\text{O}_3$  contents, assuming  $\text{Fe}^{3+}/\text{Fe}_{\text{tot}} = 0.07$  at 29 wt.% MgO (initial liquid) and  $\text{Fe}^{3+}/\text{Fe}_{\text{tot}} = 0$  at 51 wt.% MgO (olivine), was used (Table 1). The parameterization of Toplis (2005) was adopted for the Fe/Mg exchange coefficient  $K_D = (\text{Fe}^{2+}/\text{Mg})_{\text{Ol}} / (\text{Fe}^{2+}/\text{Mg})_{\text{Liq}}$ . Partitioning of minor elements in olivine was not treated explicitly. Instead, the concentrations of these elements in olivine at each increment were calculated using correlations between  $\text{Al}_2\text{O}_3$ ,  $\text{Cr}_2\text{O}_3$ , NiO, MnO, CaO and Mg# measured in olivine from Alexo by Sobolev et al.

(2007). For MgO, most samples plot near the trend of fractional crystallization (Fig. 3A), indicating that little Mg was gained by or lost from the samples, except possibly for M713 and M667. For FeO\*, the liquid line of descent displays some curvature and olivine FeO content ranges from 5 to 11 wt% (Fig. 3B). Mixing lines between evolved magmas and olivine cover a significant space in the Al<sub>2</sub>O<sub>3</sub>–FeO diagram. The forsterite content of olivine in various parts of the flow varies from Fo94 to Fo86, with an average composition around Fo92 that probably represents the composition of accumulated olivine. Low FeO\* in samples M712 and M713 is consistent with significant Fe-loss from the cumulate part of the flow (Lahaye and Arndt, 1996). For other samples, assessing the effect of secondary alteration is less straightforward.

Because of these caveats, use of Mn/Fe<sup>2+</sup>\* vs. Al/Fe<sup>2+</sup>\* diagram was explored to diagnose alteration of Fe isotopes after emplacement. In magmatic systems, Mn and Fe<sup>2+</sup> have similar crystal chemistry (similar ionic radii and identical charges) and are difficult to decouple. This is shown in Fig. 6, where the Mn/Fe<sup>2+</sup> ratio (used as a tracer of alteration) is plotted as a function of Al/Fe<sup>2+</sup>\* (used as a tracer of fractional crystallization of olivine). Olivine has Mn/Fe<sup>2+</sup>\* ratios close to the initial liquid, so that fractional crystallization cannot change much the Mn/Fe<sup>2+</sup> ratio of the melt. In contrast, in aqueous fluids, Fe<sup>2+</sup> and Mn<sup>2+</sup> have different behaviors and can easily be decoupled. Another virtue of that diagram is that mixing is represented by straight line. A third of the bulk samples (7 of 20, M666, M662, M663, M651, M655, M665, M657) plot on the magmatic evolution line. The remaining 13 bulk samples (M667, M652, M653, M654, M656, M668, AX105,

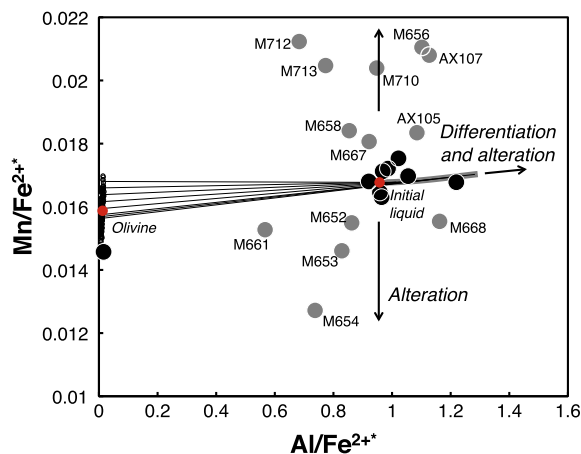


Fig. 6. Indicators of komatiite alteration and differentiation. Mn<sup>2+</sup> and Fe<sup>2+</sup>\* (calculated from FeO\*, Table 1) have very similar chemical behaviors during magmatic differentiation. Olivine has Mn<sup>2+</sup>/Fe<sup>2+</sup>\* similar to the initial melt composition. Thus, fractional crystallization of olivine in Alexo flow cannot fractionate significantly Mn<sup>2+</sup>/Fe<sup>2+</sup>\* ratios. Mixing relationships in this diagram are represented by straight lines. The 13 samples that plot off of the magmatic differentiation trend (filled gray circles, M667, M652, M653, M654, M656, M668, AX105, AX107, M658, M661, M713, M712) must have been affected by Fe and Mn mobilization and their  $\delta^{56}\text{Fe}$  values may have been modified by secondary alteration after emplacement.

AX107, M658, M710, M661, M713, M712) plot off this line and must have been affected by alteration and mobilization of Mn and Fe after emplacement of the flow. In some cases the aberrant samples are more altered than average: M652, M653, M654 and M658 are rodingitized, and samples M661, M667 and M713 are completely hydrated. However, M712 retains abundant fresh olivine yet it too plots well above the magmatic line.

Taking the data of all 20 analyzed bulk samples together, the  $\delta^{56}\text{Fe}$  value has a standard deviation of 0.056‰. If one restricts the data set to the 7 bulk samples that are on the trend of magmatic differentiation in Mn/Fe<sup>2+</sup>\* vs. Al/Fe<sup>2+</sup>\* diagram, the standard deviation decreases to 0.033. Thus, alteration is responsible for most of the isotopic fractionation documented for Fe in the flow. The Mg and Fe isotopic compositions of the bulk magma prior to alteration are calculated in Fig. 7. In the case of Mg, all bulk data are considered as nothing distinguishes chemically the two outliers AX105 and M710 from other samples. For Fe, only the bulk samples that plot on or near the magmatic evolution curve in Fig. 6 are considered. Regressions interpolated at 29.1 wt% MgO (Fig. 7) yield  $\delta^{25}\text{Mg} = -0.138 \pm 0.021\text{‰}$ ,  $\delta^{26}\text{Mg} = -0.275 \pm 0.042\text{‰}$ ,  $\delta^{56}\text{Fe} = +0.044 \pm 0.030\text{‰}$ , and  $\delta^{57}\text{Fe} = +0.059 \pm 0.044\text{‰}$ . These represent the best estimates of the isotopic composition of the erupted magma, prior to alteration. The light Fe isotopic composition of the separated olivine is discussed later.

#### 4.2. Constraints on Soret diffusion

The petrography and crystal chemistry of pyroxenes in komatiite lavas are complex and can potentially provide useful constraints on the conditions of crystallization (e.g., Fleet and MacRae, 1975; Kinzler and Grove, 1985; Parman et al., 1997; Bouquain et al., 2009). Crystallization sequences in different parts of the flow at Alexo are difficult to explain based on phase diagrams. In olivine–quartz–clinopyroxene pseudo-ternary diagram, the bulk composition of the flow plots in a field that should crystallize olivine as the liquidus phase. The second phase to crystallize should be augite, followed by pigeonite. In the rapidly cooled uppermost part of the flow, this sequence is observed. However, in the deeper part of the spinifex layer, the crystallization sequence is instead olivine followed by pigeonite and augite. Furthermore, spinifex samples containing only pyroxene and no olivine plot in the primary phase field of olivine. Bouquain et al. (2009) examined several scenarios that could explain the inversion in the crystallization sequence of augite and pigeonite and concluded that none was satisfactory. They argued instead that pyroxene crystallized from silicate liquid that differentiated internally following thermal gradients. Komatiites from Alexo are thought to have erupted as submarine lava flows that cooled and solidified due to heat loss at the top. In the crystal mush developed during magma crystallization, thermal gradients could have been sufficiently long-lived for Soret steady state to be established. Under such conditions, Mg, Fe, Al, and Ca would have migrated towards the cold end (top) while Si, Na, and K would have migrated towards

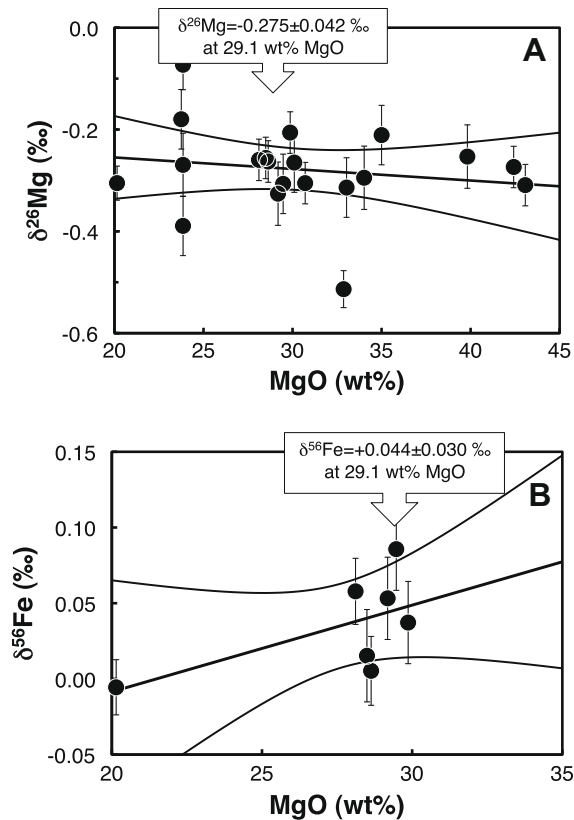


Fig. 7. Estimation of pre-alteration, pre-differentiation  $\delta^{26}\text{Mg}$  (A) and  $\delta^{56}\text{Fe}$  (B) values. Variations in MgO content reflect fractional crystallization of olivine. There are no correlations between this proxy and  $\delta^{26}\text{Mg}$  and  $\delta^{56}\text{Fe}$ . For  $\delta^{26}\text{Mg}$ , all bulk samples are plotted, as there is no clear indication that komatiite alteration affected Mg isotopic ratios. For  $\delta^{56}\text{Fe}$ , only the 7 bulk samples that plot on a trend of magmatic differentiation in  $\text{Mn}/\text{Fe}^{2+}$  vs  $\text{Al}/\text{Fe}^{2+}$  diagram (Fig. 6) are plotted. Interpolation at  $\text{MgO} = 29.1$  wt% gives for the composition of the bulk komatiite lava at emplacement  $\delta^{25}\text{Mg} = -0.138 \pm 0.021$ ‰,  $\delta^{26}\text{Mg} = -0.275 \pm 0.042$ ‰,  $\delta^{56}\text{Fe} = +0.044 \pm 0.030$ ‰, and  $\delta^{57}\text{Fe} = +0.059 \pm 0.044$ ‰.

the hot end (bottom) (Walker et al., 1988; Lesher and Walker, 1988). At the hot end, the liquid composition could have crossed the tie line that separates augite and pigeonite stability fields to first crystallize pigeonite. A long-standing difficulty with Soret diffusion, recognized early on by Bowen (1921, 1928), is that the timescale for heat conduction is almost always much faster than chemical diffusion so that temperature gradients are expected to be dissipated before elements can diffuse. The crust of a thick komatiite flow is potentially well suited for Soret diffusion to develop, however, because a strong and near-constant temperature gradient can be established in the crystal mush (Bouquain et al., 2009) and maintained for significant time as the solidification front migrates downwards towards the flow interior. For Soret effect to play a role, the presence of water at the level of  $\sim 0.3$  wt% would be required to increase the rate of chemical diffusion.

It was recognized recently that Soret effect in magmatic systems is associated with large isotopic fractionation, which could therefore be used to test for the presence of

such effects in natural systems (Richter et al., 2008, 2009a,b). Richter et al. (2009b) carried out laboratory experiments in which they placed molten basalt in a temperature gradient of  $160$  °C/cm. After the system reached Soret steady-state, the isotopic compositions of Mg, Ca, Fe, Si, and O were measured along a profile parallel to the temperature gradient. All elements showed large isotopic fractionations corresponding to enrichments in the heavy isotopes at the cold end. From the cold end to the hot end of the experimental charge, the  $\delta^{26}\text{Mg}$  and  $\delta^{56}\text{Fe}$  values varied over  $\sim 8.6$ ‰ and  $\sim 2.6$ ‰, respectively. There was a very well defined linear correlation in these experiments between  $\delta^{56}\text{Fe}$  (y) and  $\delta^{26}\text{Mg}$  (x) characterized by a slope of 0.298. In magmatic rocks, equilibrium processes like partial melting and fractional crystallization can induce variations of at most a few tenths of permil (Beard and Johnson, 2004, 2007; Williams et al., 2004, 2005; Poitrasson and Freyrier, 2005; Weyer et al., 2005; Schoenberg and von Blanckenburg, 2006; Weyer and Ionov, 2007; Heimann et al. 2008; Teng et al., 2008; Schoenberg et al., 2009; Schuessler et al., 2009; Dauphas et al., 2009a). By comparison, the Richter effect (isotopic fractionation associated with Soret effect in silicate liquids) is more than an order of magnitude larger and provides a useful proxy for recognizing such diffusion driven by thermal gradients in nature. In the mush zone of a thick komatiitic basaltic flow, Bouquain et al., 2009 estimated that the temperature gradient should be approximately  $3.2$  °C/cm over a distance of 22 cm, corresponding to a difference in temperature between the cold end and hot end of  $70$  °C. If Soret steady state were established over such a temperature difference, one would expect to find a  $1.5$ ‰ difference in  $\delta^{56}\text{Fe}$  between the hot and cold ends. For Mg, the difference in  $\delta^{26}\text{Mg}$  would be  $\sim 5.0$ ‰. As illustrated in Fig. 8, the isotopic compositions of Mg and Fe show a limited range of variations. All samples with no obvious evidence for secondary Fe mobilization (i.e., with magmatic  $\text{Mn}/\text{Fe}^{2+}$  ratio) have  $\delta^{56}\text{Fe}$  values within  $0.09$ ‰ (if one includes all bulk data, the range increases to  $0.21$ ‰). Similarly, all samples have  $\delta^{26}\text{Mg}$  values within  $0.21$ ‰ ( $0.44$ ‰ if one includes two outliers).

We propose two alternative interpretations of these results: the first is that they indicate that Soret steady state was not established in any portion of the Alexo komatiite flow. In this case, another explanation must be found for the early crystallization of pigeonite relative to augite in spinifex samples. The other explanation is that Soret diffusion might have operated to fractionate both major element and isotopes, but the effects were not preserved in the solidified samples. Fig. 9 shows the situation within the partially crystallized spinifex-textured crust of the flow. Large, vertically oriented olivine crystals separated by thin panels of liquid are growing downward towards the interior of the flow. Soret diffusion is established within the liquid panels and it enriches the hot end in Si (eventually to promote the crystallization of pyroxene) and in the light isotopes of Mg and Fe. The liquid at the cold end of the liquid panels has heavy isotopic compositions. The tips of the olivine become enriched in light Mg and Fe but the border of these grains, and the interstitial liquid, acquires a heavy isotopic composition. As the crystallization front migrates downwards, it

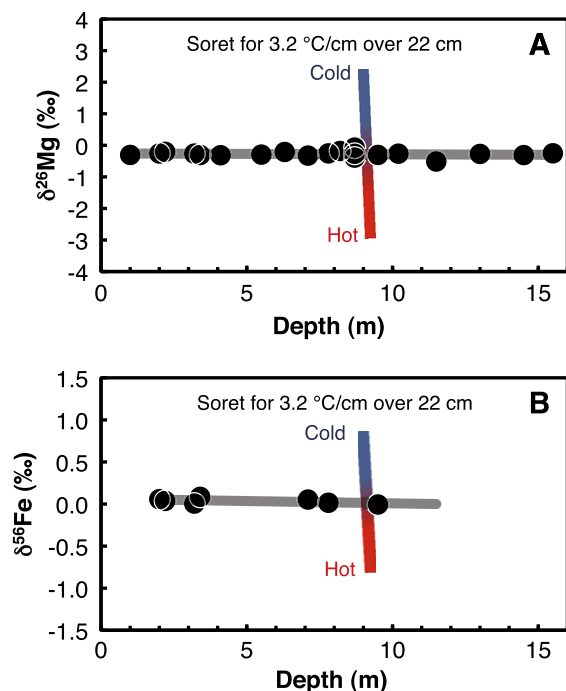


Fig. 8. Test for the presence of Soret effect in komatiites from Alexo. If Soret steady state was established for a gradient of 3.2 °C/cm over 22 cm ( $\Delta T = 70$  °C; Bouquain et al., 2009), then Mg and Fe isotopic variations of several permil would be expected between the cold and hot ends (Richter et al., 2008, 2009a,b). These variations are not observed, demonstrating the absence of Soret effect in the komatiite flow.

produces a rock containing olivine crystals that are zoned with light cores and heavy margins, but if no liquid is rejected from the mush zone, the bulk composition of individual samples will be unfractionated. We plan to test these ideas using in-situ analyses of well-preserved samples.

#### 4.3. A new tool to identify diffusive transport in zoned minerals

The low  $\delta^{56}\text{Fe}$  value ( $-0.316 \pm 0.034$ ‰) measured in olivine from cumulate sample M712 is unlikely to reflect equilibrium fractionation. Indeed, there is no evidence in bulk rock data that isotopically light olivine was removed from the system during fractional crystallization (Fig. 4). Very negative and variable  $\delta^{56}\text{Fe}$  values were also found in olivine from the Kilauea Iki lava lake (down to  $-1.1$ ‰, Teng et al., 2008).

Arndt (1986) documented the presence of zoned olivine in komatiites at Alexo. The typical profile is a decrease of the Fo content from core to rim (see Fig. 4 of Arndt, 1986). Arndt (1986) calculated the diffusion length scale for samples at different depths in the flow and concluded that significant diffusive Fe–Mg exchange could have taken place in deeply buried olivine. In silicate liquids (Richter et al., 2009a,b) and presumably in olivine as well, the light isotopes of Mg and Fe tend to diffuse faster than heavier ones. If some Mg diffused out and Fe diffused in olivine, the expectation is that olivine should have heavy Mg and light Fe isotopic compo-

sitions. The fluxes of Fe and Mg are identical in magnitude but opposite in directions. Because olivine contains more Mg than Fe (by a factor of  $\sim 10$ ), the diffusing atoms of Mg are mixed with a larger background of normal Mg than for Fe and the expected isotopic effect is smaller. However, this is partially compensated by the fact that the relative mass difference between  $^{24}\text{Mg}$  and  $^{26}\text{Mg}$  (8.3%) is a factor of 2 larger than that between  $^{54}\text{Fe}$  and  $^{56}\text{Fe}$  (3.7%). This is analogous to what was discussed in the context of Fe–Ni interdiffusion during formation of the Widmanstätten pattern in iron meteorites (Dauphas, 2007; Cook et al., 2007). The isotopic measurements made on olivine separated from M712 are qualitatively consistent with isotopic fractionation due to diffusive exchange of Mg and Fe in olivine (Fe shows large fractionation and is isotopically light while Mg shows no significant fractionation). To explore that possibility quantitatively, the isotopic effect of Fe–Mg interdiffusion in olivine was modeled using Mathematica (the program is given in Electronic annex). Because Fe–Mg diffusion coefficient is not constant, the partial differential equation that governs Fe–Mg interdiffusion in olivine has to be solved using numerical methods. The partial differential equation and the relevant initial and boundary conditions for spherical diffusion are:

$$\begin{cases} \frac{\partial C}{\partial t} = \frac{1}{r^2} \frac{\partial}{\partial r} (r^2 D \frac{\partial C}{\partial r}) \\ C(0, r) = C_0 \\ C(t, a) = C_1 \\ \left. \frac{\partial C(t, r)}{\partial r} \right|_{r=0} = 0 \end{cases},$$

where  $a$  is the grain radius,  $C_0$  is the initial concentration in olivine,  $C_1$  is the surface concentration (fixed), and the last equation corresponds to a no flux boundary condition at the center. The diffusion coefficient varies with temperature, pressure, oxygen fugacity, and the forsterite content of olivine following the parameterization of Dohmen and Chakraborty (2007). Temperature varies with time following a linear model (e.g., Arndt, 1986), the pressure is taken to be  $10^5$  Pa (1 atm), the oxygen fugacity is assumed to be at the nickel-nickel oxide buffer (Canil et al., 1994) corresponding an absolute  $f\text{O}_2$  that varies with temperature (Huebner and Sato, 1970; Chou 1987; Herd 2008) and hence time, the forsterite content of olivine is obtained by solving the partial differential equation. The diffusion coefficients of two isotopes are related by  $D_2/D_1 = (m_1/m_2)^\beta$  with  $\beta \approx 0.05$  for both Mg and Fe (Richter et al., 2009b). This value for  $\beta$  was measured experimentally for diffusion in silicate melts and it remains to be determined for diffusion in olivine. In order to assess the accuracy of the numerical solution, an isothermal calculation with constant diffusion coefficient was performed. This problem has a simple series solution (Crank, 1970),

$$C = C_0 + (C_1 - C_0) \times \left[ 1 + \frac{2a}{\pi r} \sum_{n=1}^{\infty} \frac{(-1)^n}{n} \times \sin \frac{n\pi r}{a} e^{-Dn^2\pi^2 t/a^2} \right].$$

The results of the two calculations (i.e., numerical and analytic) are strictly identical (a comparison is provided in Electronic annex).

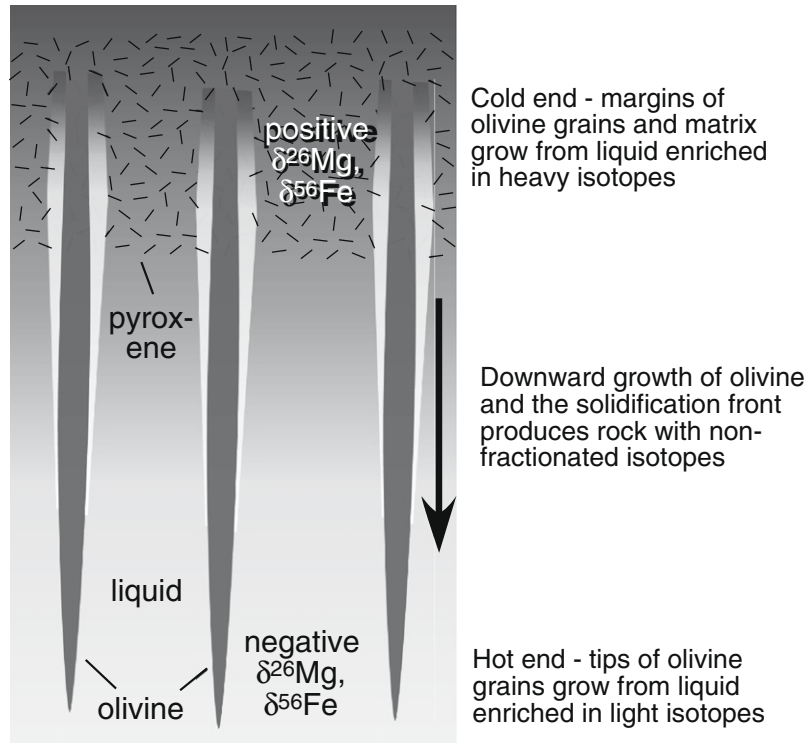


Fig. 9. Sketch illustrating how the liquid in between spinifex olivine grains may become fractionated due to the Soret effect and how downward migration of the crystallization front might eliminate the effect of this fractionation in the solidified rock. The thickness of the mush zone in the Alexo flow was probably between 20 and 50 cm.

For the purpose of evaluating the potential effect of Fe–Mg interdiffusion in olivine, we used the characteristics of an olivine grain from M676 (11 m depth) studied by Arndt (1986). It has a radius of  $\sim 300 \mu\text{m}$  with initial and surface Fo contents of 94 and 89, respectively (Fig. 4c of Arndt, 1986). The cooling rate was adjusted to  $\sim 30 \text{ K/d}$  in order to reproduce the Fo profile measured by Arndt (1986). Based on a model of conductive cooling of a lava flow, Arndt (1986) estimated a minimum cooling-rate for that sample of  $2 \text{ K/d}$ .

The computed isotopic profiles are presented in Fig. 10. As expected, Mg and Fe have heavy and light isotopic compositions relative to the bulk, respectively. Because of lower Fe concentration relative to Mg in olivine, the diffusive effects are more pronounced for Fe than for Mg. However, this is partially offset by the smaller relative mass difference of Fe isotopes relative to Mg. The  $\delta^{56}\text{Fe}:\delta^{26}\text{Mg}$  ratio in the model output ranges from  $-7:1$  to  $-4:1$ , which corresponds to the expected ratio for binary diffusion:

$$\frac{\delta^{56}\text{Fe}}{\delta^{26}\text{Mg}} \approx -\frac{\beta_{\text{Fe}}}{\beta_{\text{Mg}}} \frac{(56/54 - 1)}{(26/24 - 1)} \frac{X_{\text{Fo}}}{1 - X_{\text{Fo}}} \approx -5.$$

As the temperature decreases, the interdiffusion coefficient decreases and the system stops evolving. The final olivine is expected to have  $\delta^{56}\text{Fe} \approx \delta^{56}\text{Fe}_{\text{bulk}} - 0.23\text{‰}$  and  $\delta^{26}\text{Mg} \approx \delta^{26}\text{Mg}_{\text{bulk}} + 0.05\text{‰}$ , which is approximately consistent with the measured composition in olivine from M712. Thus, it is likely that some of the zoning documented in olivine from Alexo komatiite was created by diffusive transport of Fe and Mg.

Mineral zoning can arise from crystallization and attendant magmatic evolution, in which case the zoning profile does not provide any constraint on cooling rates. Such zoning should be associated with little isotopic fractionation as it is controlled by equilibrium isotopic fractionation at the interface between olivine and melt. Mineral zoning can also be produced by diffusive spread of sharp chemical interfaces, which should be associated with large kinetic isotope fractionation for Mg and Fe with a correlation between  $\delta^{56}\text{Fe}$  and  $\delta^{26}\text{Mg}$  of slope  $-5:1$ . Thus, isotopes allow us to unambiguously identify diffusive transport in zoned minerals, which is key to constraining magmatic timescales (Fig. 11, Dauphas, 2007; Watson and Baxter, 2007; Costa et al., 2008, and references therein).

#### 4.4. Clues from komatiites on the Mg and Fe isotopic compositions of the silicate Earth

The Mg and Fe isotopic compositions of the silicate Earth have been debated. Wiechert and Halliday (2007) proposed a  $\delta^{26}\text{Mg}$  value of  $-0.06 \pm 0.03\text{‰}$  for the Earth, which is significantly heavier than the chondritic value of approximately  $-0.3\text{‰}$ . They interpreted the non-chondritic Mg isotopic composition of the Earth as due to sorting of chondrule-size material in the solar nebula. However, subsequent high precision analyses of mantle peridotites and basalts revealed that the Earth most likely has chondritic Mg isotopic composition (Teng et al., 2007, 2010; Handler et al., 2009; Yang et al., 2009). Given that most Mg resides in the mantle, the BSE Mg isotopic composition is represen-

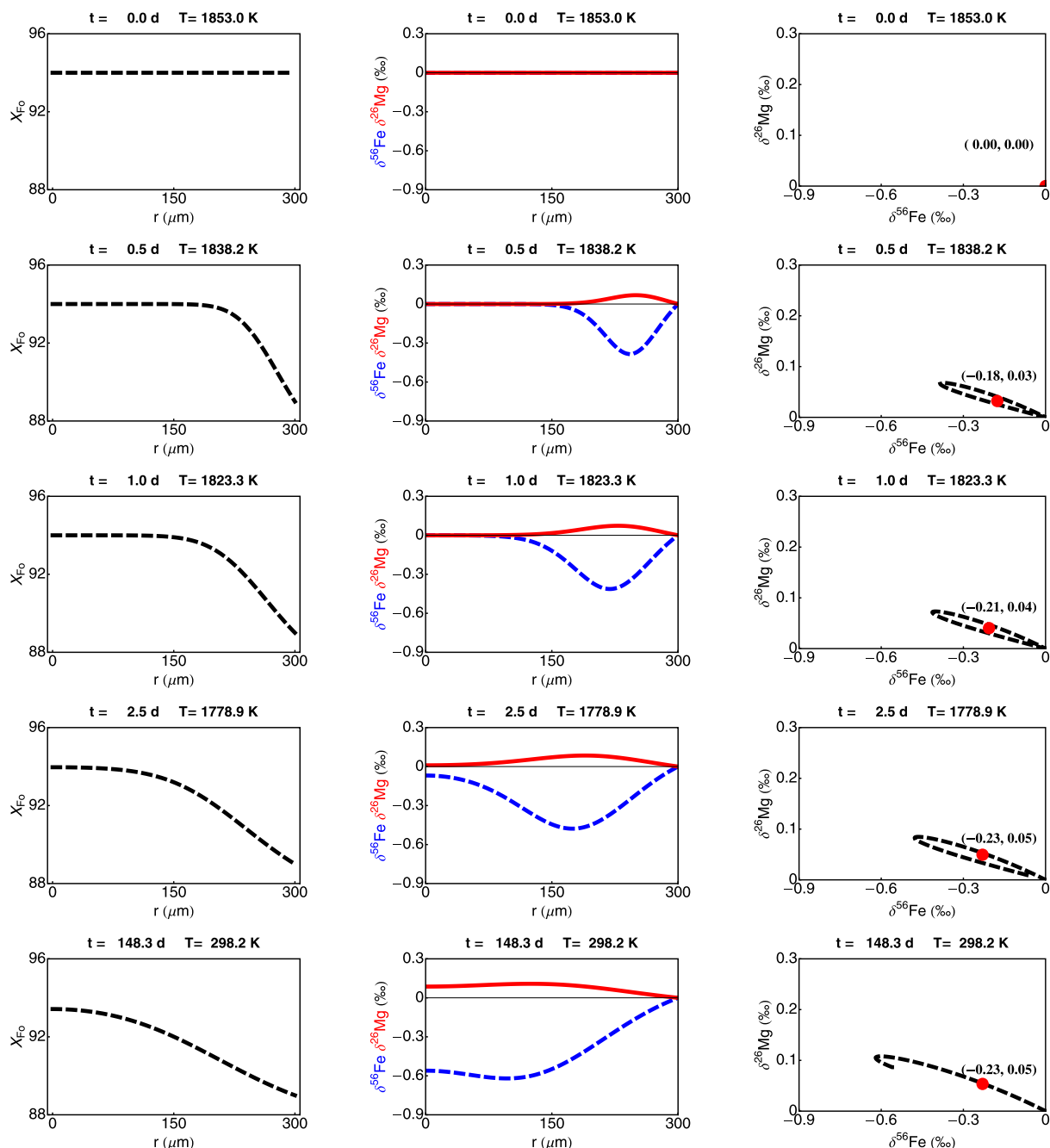


Fig. 10. Modeling of isotopic fractionation associated with Fe–Mg interdiffusion in olivine (the Mathematica code and an animated gif version of this figure are available in [Electronic annex](#)). An early-formed crystal of olivine of 300  $\mu\text{m}$  radius and Fo94 is placed in a more evolved liquid corresponding to olivine Fo89. The system evolves towards equilibrium by outward diffusion of Mg and inward diffusion of Fe, resulting in heavy Mg and light Fe isotopic compositions in the crystal (lighter isotopes tend to diffuse faster than heavier ones; [Richter et al., 2009a,b](#)). The fluxes of Mg and Fe are identical in magnitude but opposite in directions. Because olivine contains more Mg than Fe, the isotopic fractionation for Mg is smaller than for Fe due to dilution effects (in a ratio  $\sim 5:1$ , also see, [Dauphas, 2007](#)). During cooling (at 30 K/d), the Fe–Mg interdiffusion coefficient decreases and the system freezes at around 1,500  $^{\circ}\text{C}$ . The left column shows evolution of the Fo content versus radial distance, the middle column shows  $\delta^{26}\text{Mg}$  (solid red) and  $\delta^{56}\text{Fe}$  (dashed blue) versus radial distance, and the right column shows  $\delta^{26}\text{Mg}$  versus  $\delta^{56}\text{Fe}$  (the red dot and the two numbers in parentheses are the bulk compositions of olivine calculated using  $\delta_{\text{bulk}} = \int_0^a \delta(r) C(r) r^2 dr / \int_0^a C(r) r^2 dr$ ). Time (in days) and temperature (in K) are given above each panel.  $D_{\text{Mg,Fe}}$  was calculated using the parameterization of [Dohmen and Chakraborty \(2007\)](#). It depends to temperature (variable), pressure ( $P = 10^5$  Pa), Fo content of olivine (output from the computation) and oxygen fugacity (NNO oxygen buffer, [Huebner and Sato, 1970](#); [Chou, 1987](#); [Canil et al., 1994](#); [Herd, 2008](#)). For diffusive fractionation of isotopes,  $\beta_{\text{Mg,Fe}} = 0.05$  was used (no data is available for solid silicates, so the value measured in liquid silicates by [Richter et al. \(2009b\)](#) was used instead). See text for details. (For interpretation of the references to color in this figure legend, the reader is referred to the web version of this paper.)

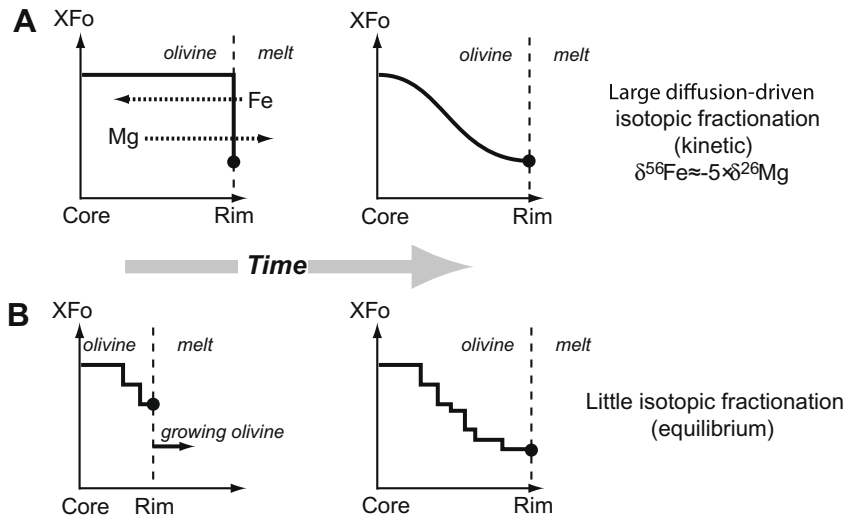


Fig. 11. Illustration of how isotopes can be used to identify diffusive transport in zoned minerals. In the top panel (a), olivine starts with homogenous Fo content. A change in condition at the surface induces inward diffusion of Fe and outward diffusion of Mg. As discussed in the text, such diffusive transport is associated with kinetic fractionation characterized by  $\delta^{56}\text{Fe}/\delta^{26}\text{Mg} \approx -5$ . In the bottom panel (b), olivine grows from an evolving liquid. No diffusive transport is associated with mineral zoning and olivine should show little Mg and Fe isotopic fractionation. In both cases, the chemical zoning are similar but only (a) will show large isotopic fractionation associated with diffusion.

tative of the bulk Earth composition. The iron isotopic composition of the BSE has also been the subject to some controversy. It was recognized early on that chondrites have a homogeneous Fe isotopic composition ( $\delta^{56}\text{Fe} \sim 0\text{‰}$ ; Poirasson et al., 2005; Schoenberg and von Blanckenburg, 2006; Dauphas and Rouxel, 2006; Dauphas et al., 2009a) and that MORBs and OIBs are isotopically heavy relative to chondrites ( $\delta^{56}\text{Fe} \sim +0.1\text{‰}$ ) (Beard et al., 2003; Poirasson et al., 2004; Schoenberg and von Blanckenburg, 2006; Weyer and Ionov, 2007; Teng et al., 2008; Schuessler et al., 2009). If these elevated  $\delta^{56}\text{Fe}$  values are representative of the BSE, two interpretations can be envisioned. Poirasson et al. (2004) proposed that Fe was vaporized during the Moon-forming impact, which enriched the residue in the heavy isotopes. More recently, Polyakov (2009) argued that this was the imprint of high-pressure, high-temperature equilibrium isotopic fractionation between mantle and core. However, peridotite data show that iron isotopes can be fractionated during partial melting (Williams et al., 2004, 2005; Weyer et al., 2005; Weyer and Ionov, 2007). Weyer and Ionov (2007) found a statistically significant correlation between  $\delta^{56}\text{Fe}$  and Mg#, a proxy of degree of melt extraction. When interpolated to the Mg# of the fertile mantle (89.4), the  $\delta^{56}\text{Fe}$  value of the BSE is estimated to be  $+0.02 \pm 0.03\text{‰}$ . They thus proposed that the heavy iron isotopic composition of basalts could result from isotopic fractionation during partial melting. Beard and Johnson (2007) and Poirasson (2007) disputed this interpretation on the basis that basalts from Mars and Vesta do not show such fractionation and that mantle peridotites sample the lithosphere whereas basalts largely record the composition of the asthenosphere (however see Weyer et al., 2007). More recently, Dauphas et al. (2009a) reported the discovery of IABs and boninites with near-chondritic Fe isotopic compositions. In particular, Eoarchean and modern boninites, which formed by large degree partial melting of de-

pleted mantle sources, show a very narrow range of  $\delta^{56}\text{Fe}$  values centered at  $+0.028 \pm 0.008\text{‰}$ . The observed variations are best explained by the BSE having a near-chondritic iron isotopic composition with  $\sim +0.3\text{‰}$  equilibrium isotope fractionation between  $\text{Fe}^{3+}$  and  $\text{Fe}^{2+}$  during mantle melting, and preferential extraction of isotopically heavier, incompatible  $\text{Fe}^{3+}$ .

Komatiites are particularly well suited for characterizing the Mg and Fe isotopic compositions of the mantle because they correspond to high degree partial melts ( $\sim 50\%$  in the case of Alexo; Arndt, 2003), as opposed to  $\sim 10\%$  partial melting for MORBs (Klein and Langmuir, 1987). As a result, their isotopic compositions should be closer to the source composition than for MORBs. How close is a matter of uncertainty as it depends on the mechanism that governs iron isotopic fractionation during partial melting (i.e., fractionation between  $\text{Fe}^{2+}$  and  $\text{Fe}^{3+}$  or fractionation between Fe in solid and melt; Weyer and Ionov, 2007; Dauphas et al., 2009a). They formed at near neutral buoyancy, which should promote equilibration with the mantle. Finally, they formed at high temperatures, which should reduce any equilibrium isotopic fractionation ( $\propto 1/T^2$ ) and should have promoted equilibration between the melt and the residue by accelerating diffusion and dissolution/precipitation kinetics. In the case of Mg, using komatiites to estimate the composition of the silicate Earth is relatively straightforward because fractional crystallization does not fractionate Mg isotopes and basalts have  $\delta^{26}\text{Mg}$  values very similar to mantle peridotites (Teng et al., 2007, 2010; Handler et al., 2009; Yang et al., 2009). The Mg isotope values of  $\delta^{25}\text{Mg} = -0.138 \pm 0.020\text{‰}$  and  $\delta^{26}\text{Mg} = -0.274 \pm 0.040\text{‰}$  for the flow unaffected by alteration and differentiation (Fig. 7A) therefore represents an excellent proxy for the composition of the source of Alexo komatiites, possibly the Archean lower mantle. It is identical to the average value of mantle peridotites of

$\delta^{25}\text{Mg} = -0.14\text{‰}$  and  $\delta^{26}\text{Mg} = -0.27\text{‰}$  (Fig. 12, Handler et al., 2009; Teng et al., 2010). It is also very close to the chondritic composition (Fig. 12, Young and Galy, 2004; Baker et al., 2005; Wiechert and Halliday, 2007; Teng et al., 2007, 2010).

Because partial melting can fractionate iron isotopes, the  $\delta^{56}\text{Fe}$  value of the komatiite flow of  $+0.044 \pm 0.030\text{‰}$  (Fig. 7B) may not represent the mantle composition. Dauphas et al. (2009a) proposed a quantitative model that relates the Fe isotopic compositions of mantle magmas to the  $\delta^{56}\text{Fe}$  value of the source. The ingredients in this model are: (i) the equilibrium isotopic fractionation factor between  $\text{Fe}^{2+}$  and  $\text{Fe}^{3+}$ , (ii) the liquid/solid partition coefficients of  $\text{Fe}^{2+}$  and  $\text{Fe}^{3+}$ , (iii) the  $\text{Fe}^{3+}/\text{Fe}^{2+}$  ratio of the mantle source, (iv) its oxygen buffer capacity, (v) the degree of partial melting, and (vi) the mode of melting. For explaining the Fe isotopic variations measured in MORBs, OIBs, IABs, and boninites, an equilibrium fractionation between  $\text{Fe}^{3+}$  and  $\text{Fe}^{2+}$  of  $\sim +0.3\text{‰}$  is needed, which is consistent with predictions based on Mössbauer spectroscopy (Polyakov and Mineev, 2000). The fractionation between  $\text{Fe}^{3+}$  and  $\text{Fe}^{2+}$  in silicate melts is not known but as a first approach we shall assume that it is similar to silicate minerals. Komatiites probably formed in hot plumes within a mantle that was hotter than the present one. In order to account for the  $>300\text{ °C}$  higher temperature of melting of komatiites relative to MORBs, the equilibrium fractionation between  $\text{Fe}^{3+}$  and  $\text{Fe}^{2+}$  is reduced to  $+0.2\text{‰}$  (Polyakov and Mineev, 2000). The liquid/solid partition coefficients of  $\text{Fe}^{2+}$  and  $\text{Fe}^{3+}$  are taken to be 1 and 10, respectively (Canil et al., 1994). The  $\text{Fe}^{3+}/\text{Fe}^{2+}$  ratio mea-

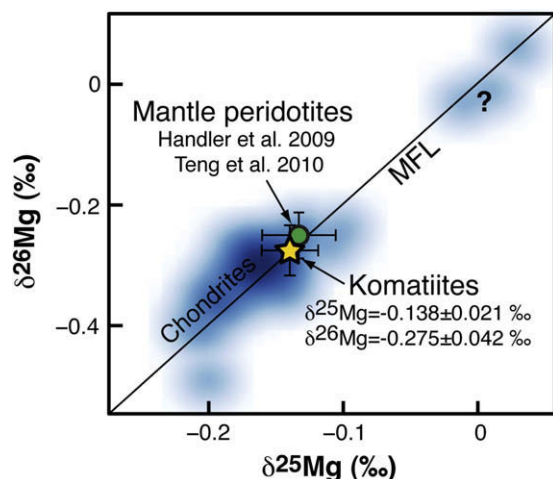


Fig. 12. Comparison between bulk komatiite (yellow star,  $\delta^{25}\text{Mg} = -0.138 \pm 0.021\text{‰}$  and  $\delta^{26}\text{Mg} = -0.275 \pm 0.042\text{‰}$ , Fig. 7A), mantle peridotite (green dot, Handler et al., 2009; Teng et al., 2010), and chondrite (blue density plot, Young and Galy, 2004; Baker et al., 2005; Wiechert and Halliday, 2007; Teng et al., 2007; Teng et al., 2010) Mg isotopic compositions. Komatiite values represent good estimates of the BSE composition. MFL stands for Mass Fractionation Line. The question mark corresponds to 3 outlier data from Young and Galy (2004) and Baker et al. (2005). (For interpretation of the references to color in this figure legend, the reader is referred to the web version of this paper.)

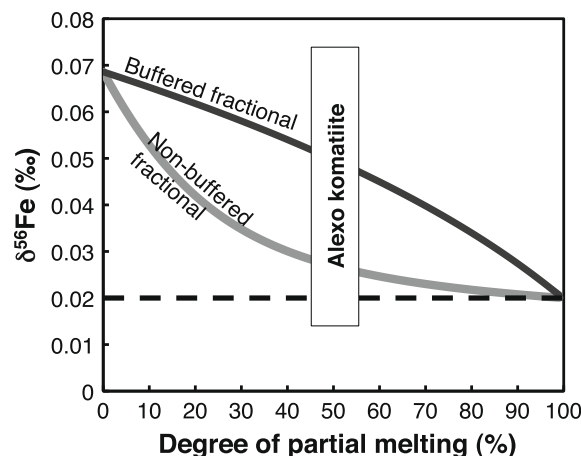


Fig. 13. Iron isotopic composition of magmas as a function of degree of partial melting for buffered (constant  $\text{Fe}^{3+}/\text{Fe}^{2+}$  ratio) and non-buffered (decreasing  $\text{Fe}^{3+}/\text{Fe}^{2+}$  ratio) melting. The  $\delta^{56}\text{Fe}$  value of the mantle source is  $\sim +0.02\text{‰}$  (Weyer and Ionov, 2007). The curves for fractional melting were calculated following the model proposed by Dauphas et al. (2009a) for redox-controlled Fe isotopic fractionation during melting. The parameters are  $(\text{Fe}^{3+}/\text{Fe}^{2+})_0 = 0.037$ ,  $K_{\text{Fe}^{2+}}^{l/s} = 1$ ,  $K_{\text{Fe}^{3+}}^{l/s} = 10$  (Canil et al., 1994), and  $\Delta\text{Fe}^{3+} - \text{Fe}^{2+} = 0.2\text{‰}$  (see text for details). The box labeled “Alexo Komatiite” represents the locus of the primary magma (50% partial melting and  $\delta^{56}\text{Fe} = +0.044 \pm 0.030\text{‰}$ ) (Fig. 7B).

sured in melt inclusions from 2.7 Ga komatiite from Belingwe is consistent with near-anhydrous melting of a source with similar iron oxidation state as MORBs (Berry et al., 2008). It is therefore assumed that komatiites formed from a source with a  $\text{Fe}^{3+}/\text{Fe}^{2+}$  ratio identical to that of the fertile mantle (0.037; Canil et al., 1994). It is difficult to determine to what extent the oxygen fugacity was buffered during melting. Trace element data indicate that Munro-type komatiites formed by 50% partial melting under fractional melting conditions (Arndt, 2003). Using the equations derived by Dauphas et al. (2009a), the Fe isotopic composition of komatiite magma was calculated as a function of degree of partial melting for conditions of buffered and non-buffered oxygen fugacity. At 50% partial melting of a source with  $\delta^{56}\text{Fe} = +0.02\text{‰}$ , one would expect the iron isotopic composition of the magmas to be between  $+0.027\text{‰}$  (non-buffered) and  $+0.050\text{‰}$  (buffered) (Fig. 13). This is in very good agreement with the measured composition of  $+0.044 \pm 0.030\text{‰}$ . Such a composition would be impossible to produce from a mantle with a  $\delta^{56}\text{Fe}$  of  $+0.1\text{‰}$ . These results therefore support the view of Weyer and Ionov (2007) and Dauphas et al. (2009a) that the BSE has near-chondritic  $\delta^{56}\text{Fe}$  (i.e.,  $+0.044 \pm 0.030\text{‰}$ ).

## 5. CONCLUSIONS

Komatiites from Alexo are relatively well preserved and represent high degree partial melts ( $\sim 50\%$ ). They are thus well suited for investigating the Mg and Fe isotopic compositions of the Archean mantle and the conditions of magmatic differentiation of ultramafic lavas. High precision Mg and Fe isotopic analyses of 22 samples taken along a

15-m depth profile in a komatiite flow (Table 2 and Fig. 1) are reported, from which the following conclusions can be reached:

1. Iron isotopic composition varies beyond the range of analytical uncertainty. Several samples do not plot on a trend of olivine-controlled magmatic differentiation in a  $\text{Mn}/\text{Fe}^{2+}$  vs.  $\text{Al}/\text{Fe}^{2+}$  diagram, reflecting secondary mobilization of iron (Fig. 6). If these samples are excluded, the remaining 7 bulk samples give pre-alteration, pre-differentiation  $\delta^{56}\text{Fe}$  and  $\delta^{57}\text{Fe}$  values for the bulk flow of  $+0.044 \pm 0.030\text{‰}$ , and  $+0.059 \pm 0.044\text{‰}$ , respectively (Fig. 7B). These values are lower than those measured in MORBs and OIBs, which is consistent with the idea that komatiites represent high degree partial melts. These results also support the view that the silicate Earth has near-chondritic Fe isotopic composition (i.e.,  $\delta^{56}\text{Fe} = +0.044 \pm 0.030\text{‰}$ ; also see Weyer and Ionov, 2007; Dauphas et al., 2009a).
2. Except for two outliers, the magnesium isotopic compositions of all komatiites from Alexo are homogeneous (Fig. 1). The  $\delta^{25}\text{Mg}$  and  $\delta^{26}\text{Mg}$  values of the bulk flow are  $-0.138 \pm 0.021\text{‰}$  and  $-0.275 \pm 0.042\text{‰}$ , respectively (Fig. 7A). These values are indistinguishable from average mantle peridotite values and represent the best estimates of the composition of the silicate Earth from analysis of volcanic rocks. These values are also identical to chondrites (Fig. 12) and support the view that the silicate Earth has chondritic Mg isotopic composition (Teng et al., 2007, 2010; Handler et al., 2009; Yang et al., 2009).
3. In order to explain the early crystallization of pigeonite relative to augite in slowly cooled spinifex lava, Bouquain et al. (2009) suggested that magma trapped in the crystal mush during spinifex growth differentiated by Soret diffusion. Soret steady-state should be associated with several permil correlated variations in the isotopic compositions of Mg and Fe. Such variations are not found in the Alexo komatiite (Fig. 8), demonstrating that Soret effect was not present during the differentiation of this flow.
4. The low  $\delta^{56}\text{Fe}$  and near-normal  $\delta^{26}\text{Mg}$  of olivine in sample M712 can be explained by diffusive exchange of Mg and Fe during cooling (Fig. 10). Isotopes thus represent a new tool to identify diffusion transport in zoned minerals (Fig. 11), which is important for estimating cooling rates and for understanding crystal growth in magmas.

#### ACKNOWLEDGMENTS

Frank M. Richter's discovery of the Richter effect (isotopic fractionation driven by thermal diffusion in silicate melts) was an inspiration for this study. Discussions with F.M. Richter, P.R. Craddock, C. Sio, M. Roskosz, W. Li, P.D. Asimow, J.M. Eiler, and E.M. Stolper were greatly appreciated. Thoughtful reviews by S. Weyer, H.M. Williams, J. Baker, as well as comments by Associate Editor M. Rehkämper improved the manuscript. This work was supported by a Packard fellowship, the France Chicago Center, a Moore Distinguished Scholarship at the California Institute of Technology, NASA and NSF through Grants

NNG06GG75G, NNX09AG59G, and EAR-0820807 to N.D and by NSF through Grant EAR-0838227 to F.Z.T.

#### APPENDIX A. SUPPLEMENTARY DATA

Supplementary data associated with this article can be found, in the online version, at doi:10.1016/j.gca.2010.02.031.

#### REFERENCES

- Arndt N. T. (1986) Differentiation of komatiite flows. *J. Petrol.* **27**, 279–301.
- Arndt N., Ginibre C., Chauvel C., Albarède F., Cheadle M., Herzberg C., Jenner G. and Lahaye Y. (1998) Were komatiite wet? *Geology* **26**, 739–742.
- Arndt N. (2003) Komatiites, kimberlites, and boninites. *J. Geophys. Res.* **108**(B6), 2293. doi:10.1029/2002JB002157.
- Arndt N. and Leshar C. M. (2004) Komatiite. In *Encyclopedia of Geology* (eds. D. Selle, R. Cocks and I. Plimer). Elsevier, Amsterdam, pp. 260–268.
- Baker J. A., Bizzarro M., Wittig N., Connelly J. and Haack H. (2005) Early planetesimal melting from an age of 4.5662 Gyr for differentiated meteorites. *Nature* **436**, 1127–1131.
- Barnes S. J., Gorton M. P. and Naldrett A. J. (1983) A comparative study of olivine and clinopyroxene spinifex flows from Alexo, Abitibi greenstone belt, Canada. *Contrib. Mineral. Petrol.* **83**, 293–308.
- Beard B. L., Johnson C. M., Skulan J. L., Nealson K. H., Cox L. and Sun H. (2003) Application of Fe isotopes to tracing the geochemical and biological cycling of Fe. *Chem. Geol.* **195**, 87–117.
- Beard B. L. and Johnson C. M. (2004) Inter-mineral Fe isotope variations in mantle-derived rocks and implications for the Fe geochemical cycle. *Geochim. Cosmochim. Acta* **68**, 4727–4743.
- Beard B. L. and Johnson C. M. (2007) Comment on "Iron isotope fractionation during planetary differentiation" by S. Weyer et al., *Earth Planet. Sci. Lett.* V240, pages 251–264". *Earth Planet. Sci. Lett.* **256**, 633–637.
- Beattie P. (1993) Olivine-melt and orthopyroxene-melt equilibria. *Contrib. Mineral. Petrol.* **115**, 103–111.
- Bekker A., Barley M. E., Fiorentini M. L., Rouxel O. J., Rumble D. and Beresford S. W. (2009) Atmospheric sulfur in Archean komatiite-hosted nickel deposits. *Science* **326**, 1086–1089.
- Berry A. J., Danyushevsky L. V., O'Neill H. St. C., Newville M. and Sutton S. R. (2008) Oxidation state of iron in komatiitic melt inclusions indicates hot Archean mantle. *Nature* **455**, 960–963.
- Bouquain S., Arndt N. T., Hellebrand E. and Faure F. (2009) Crystallochemistry and origin of pyroxenes in komatiites. *Contrib. Mineral. Petrol.* **158**, 599–617.
- Bowen N. L. (1921) Diffusion in silicate melts. *J. Geol.* **29**, 295–317.
- Bowen N.L. (1928) *The Evolution of the Igneous Rocks*. Princeton University Press.
- Brantley S. L., Liermann L. J., Guynn R. L., Anbar A., Icopini G. A. and Barling J. (2004) Fe isotopic fractionation during mineral dissolution with and without bacteria. *Geochim. Cosmochim. Acta* **68**, 3189–3204.
- Canil D., O'Neill H. St. C., Pearson D. G., Rudnick R. L., McDonough W. F. and Carswell D. A. (1994) Ferric iron in peridotites and mantle oxidation states. *Earth Planet. Sci. Lett.* **123**, 205–220.
- Chou I.-M. (1987) Oxygen buffer and hydrogen sensor techniques at elevated pressures and temperatures. In *Hydrothermal*

- Experimental Techniques* (eds. G. C. Ulmer and H. L. Barnes). John Wiley & Sons, New York, pp. 61–99.
- Cook D. L., Wadhwa M., Clayton R. N., Dauphas N., Janney P. E. and Davis A. M. (2007) Mass-dependent fractionation of nickel isotopes in meteoritic metal. *Meteorit. Planet. Sci.* **42**, 2067–2077.
- Corfu F. (1993) The evolution of the southern Abitibi greenstone belt in light of precise. U–Pb geochronology. *Econ. Geol.* **88**, 1323–1340.
- Costa F., Dohmen R. and Chakraborty S. (2008) Time scales of magmatic processes from modeling the zoning patterns of crystals. *Rev. Mineral. Geochem.* **69**, 545–594.
- Crank J. (1970) *The Mathematics of Diffusion*. Oxford University Press.
- Dauphas N., Janney P. E., Mendybaev R. A., Wadhwa M., Richter F. M., Davis A. M., van Zuilen M., Hines R. and Foley C. N. (2004) Chromatographic separation and multicollection-ICPMS analysis of iron. Investigating mass-dependent and -independent isotope effects. *Anal. Chem.* **76**, 5855–5863.
- Dauphas N. and Rouxel O. (2006) Mass spectrometry and natural variations of iron isotopes. *Mass Spectrom. Rev.* **25**, 515–550. *Erratum* **25**, 831–832.
- Dauphas N. (2007) Diffusion-driven kinetic isotope effect of Fe and Ni during formation of the Widmanstätten pattern. *Meteorit. Planet. Sci.* **42**, 1597–1613.
- Dauphas N., Craddock P. R., Asimow P. D., Bennett V. C., Nutman A. P. and Ohnenstetter D. (2009a) Iron isotopes may reveal the conditions of mantle melting from Archean to present. *Earth Planet. Sci. Lett.* **288**, 255–267.
- Dauphas N., Pourmand A. and Teng F.-Z. (2009b) Routine isotopic analysis of iron by HR-MC-ICPMS: how precise and how accurate? *Chem. Geol.* **267**, 175–184.
- Dohmen R. and Chakraborty S. (2007) Erratum to “Fe–Mg diffusion in olivine II: point defect chemistry, change of diffusion mechanisms and a model calculation of diffusion coefficients in natural olivine”. *Phys. Chem. Minerals* **34**, 597–598.
- Faure F., Arndt N. and Libourel G. (2006) Formation of spinifex texture in komatiites: an experimental study. *J. Petrol.* **47**, 1591–1610.
- Fleet M. E. and MacRae N. D. (1975) A spinifex rock from Munro Township, Ontario. *J. Can. Earth Sci.* **12**, 928–939.
- Galy A., Yoffe O., Janney P. E., Williams R. W., Cloquet C., Alard O., Halicz L., Wadhwa M., Hutcheon I. D., Ramon E. and Carignan J. (2003) Magnesium heterogeneity of the isotopic standard SRM 980 and new reference materials for magnesium-isotope-ratio measurements. *J. Anal. Atom. Spectrom.* **18**, 1352–1356.
- Handler M. R., Baker J. A., Schiller M., Bennett V. C. and Yaxley G. M. (2009) Magnesium stable isotope composition of Earth's upper mantle. *Earth Planet. Sci. Lett.* **282**, 306–313.
- Heimann A., Beard B. L. and Johnson C. M. (2008) The role of volatile exsolution and sub-solidus fluid/rock interactions in producing high  $^{56}\text{Fe}/^{54}\text{Fe}$  ratios in siliceous igneous rocks. *Geochim. Cosmochim. Acta* **72**, 4379–4396.
- Herd C. D. K. (2008) Basalts as probes of planetary interior redox state. *Rev. Mineral. Geochem.* **68**, 527–553.
- Herzberg C. (1992) Depth and degree of melting of komatiites. *J. Geophys. Res.* **97**(B4), 4521–4540.
- Herzberg C., Asimow P.D., Arndt N., Niu Y., Leshner C.M., Fitton J.G., Cheadle M.J. and Saunders A.D. (2007) Temperatures in ambient mantle and plumes: Constraints from basalts, picrites, and komatiites. *Geochem. Geophys. Geosyst.* **8**, Q02006, doi:10.1029/2006GC001390.
- Huang F., Lundstrom C. C., Glessner J., Ianno A., Boudreau A., Li J., Ferré E. C., Marshak S. and DeFrates J. (2009) Chemical and isotopic fractionation of wet andesite in a temperature gradient: experiments and models suggesting a new mechanism of magma differentiation. *Geochim. Cosmochim. Acta* **73**, 729–749.
- Huebner J. S. and Sato M. (1970) The oxygen fugacity–temperature relationships of manganese oxide and nickel oxide buffers. *Am. Mineral.* **55**, 934–952.
- Icopini G. A., Anbar A. D., Ruebush S. S., Tien M. and Brantley S. L. (2004) Iron isotope fractionation during microbial reduction of iron: the importance of adsorption. *Geology* **32**, 205–208.
- Jolly W. T. (1982) Progressive metamorphism of komatiites and related Archean lavas of the Abitibi area, Canada. In *Komatiites* (eds. N. T. Arndt and E. G. Nisbet). Allen and Unwin, London, pp. 245–266.
- Kinzler R. J. and Grove T. L. (1985) Crystallization and differentiation of Archean komatiite lavas from northeast Ontario: phase equilibrium and kinetic studies. *Am. Mineral.* **70**, 40–51.
- Klein E. M. and Langmuir C. H. (1987) Global correlations of ocean ridge basalt chemistry with axial depth and crustal thickness. *J. Geophys. Res.* **92B**, 8089–8115.
- Lahaye Y., Arndt N., Byerly G., Chauvel C., Fourcade S. and Gruau G. (1995) The influence of alteration on the trace-element and Nd isotopic compositions of komatiites. *Chem. Geol.* **126**, 43–64.
- Lahaye Y. and Arndt N. (1996) Alteration of a komatiite flow from Alexo, Ontario, Canada. *J. Petrol.* **37**, 1261–1284.
- Leshner C.E. and Walker D. (1988) Cumulate maturation and melt migration in a temperature gradient. *J. Geophys. Res.* **93**, 10295–10311.
- Matsumoto T., Seta A., Matsuda J.-I., Takebe M., Chen Y. and Arai S. (2002) Helium in the Archean komatiites revisited: significantly high  $^3\text{He}/^4\text{He}$  ratios revealed by fractional crushing gas extraction. *Earth Planet. Sci. Lett.* **196**, 213–225.
- Miller G. H., Stolper E. M. and Ahrens T. J. (1991) The equation of state of molten komatiite: 2. Application to komatiite petrogenesis and the Hadean mantle. *J. Geophys. Res.* **96**, 11849–11864.
- Muir J. E. and Comba C. D. A. (1979) The Dundonald deposit: an example of volcanic-type nickel sulphide mineralization. *Can. Mineral.* **17**, 351–360.
- Naldrett A. J. and Mason G. D. (1968) Contrasting Archean ultramafic bodies in Dundonald and Clergue Townships, Ontario. *Can. J. Earth Sci.* **5**, 111–143.
- Naldrett A.J. (1979) Field guide to Alexo area. Guide Book for Sulphide Field Conference, October 1978.
- Nisbet E. G., Cheadle M. J., Arndt N. T. and Bickle M. J. (1993) Constraining the potential temperature of the Archean mantle: a review of the evidence from komatiites. *Lithos* **30**, 291–307.
- Ohtani E. (1984) Generation of komatiite magma and gravitational differentiation in the deep upper mantle. *Earth Planet. Sci. Lett.* **67**, 261–272.
- Parman S. W., Dann J. C., Grove T. L. and de Wit M. J. (1997) Emplacement conditions of komatiite magmas from the 3.49 Ga Komati Formation, Barberton greenstone belt, South Africa. *Earth Planet. Sci. Lett.* **150**, 303–323.
- Poitras F., Halliday A. N., Lee D.-C., Levasseur S. and Teutsch N. (2004) Iron isotope differences between Earth, Moon, Mars and Vesta as possible records of contrasted accretion mechanisms. *Earth Planet. Sci. Lett.* **223**, 253–266.
- Poitras F. and Frey R. (2005) Heavy iron isotope composition of granites determined by high resolution MC-ICP-MS. *Chem. Geol.* **222**, 132–147.
- Poitras F., Levasseur S. and Teutsch N. (2005) Significance of iron isotope mineral fractionation in pallasites and iron

- meteorites for the core-mantle differentiation of terrestrial planets. *Earth Planet. Sci. Lett.* **234**, 151–164.
- Poitrasson F. (2007) Does planetary differentiation really fractionate iron isotopes? *Earth Planet. Sci. Lett.* **256**, 484–492.
- Polyakov V. B. and Mineev S. D. (2000) The use of Mössbauer spectroscopy in stable isotope geochemistry. *Geochim. Cosmochim. Acta* **64**, 849–865.
- Polyakov V. B. (2009) Equilibrium iron isotope fractionation at core-mantle boundary conditions. *Science* **323**, 912–914.
- Puchtel I. S., Humayun M., Campbell A. J., Sproule R. A. and Lesher C. M. (2004) Platinum group element geochemistry of komatiites from the Alexo and Pyke Hills areas, Ontario, Canada. *Geochim. Cosmochim. Acta* **68**, 1361–1383.
- Pyke D. R., Naldrett A. J. and Eckstrand O. R. (1973) Archaean ultramafic flows in Muno Township, Ontario. *Geol. Soc. Am. Bull.* **84**, 955–978.
- Richard D., Marty B., Chaussidon M. and Arndt N. (1996) Helium isotopic evidence for a lower mantle component in depleted Archaean komatiite. *Science* **273**, 93–95.
- Richter F. M. (1985) Models for the Archaean thermal regime. *Earth Planet. Sci. Lett.* **73**, 350–360.
- Richter F. M., Watson E. B., Mendybaev R. A., Teng F.-Z. and Janney P. E. (2008) Magnesium isotope fractionation in silicate melts by chemical and thermal diffusion. *Geochim. Cosmochim. Acta* **72**, 206–220.
- Richter F. M., Dauphas N. and Teng F.-Z. (2009a) Non-traditional fractionation of non-traditional isotopes: evaporation, chemical diffusion and Soret diffusion. *Chem. Geol.* **258**, 92–103.
- Richter F. M., Watson E. B., Mendybaev R., Dauphas N., Georg B., Watkins J. and Valley J. (2009b) Isotopic fractionation of the major elements of molten basalt by chemical and thermal diffusion. *Geochim. Cosmochim. Acta* **73**, 4250–4263.
- Rouxel O., Dobbek N., Ludden J. and Fouquet Y. (2003) Iron isotope fractionation during oceanic crust alteration. *Chem. Geol.* **202**, 155–182.
- Schandl E. S., O'Hanley D. S. and Wicks F. J. (1989) Rodingites in serpentinized ultramafic rocks of the Abitibi greenstone belt, Ontario. *Can. Mineral.* **27**, 579–591.
- Schoenberg R. and von Blanckenburg F. (2006) Modes of planetary-scale Fe isotope fractionation. *Earth Planet. Sci. Lett.* **252**, 342–359.
- Schoenberg R., Marks M. A. W., Schuessler J. A., von Blanckenburg F. and Markl G. (2009) Fe isotope systematics of coexisting amphibole and pyroxene in the alkaline igneous rock suite of the Illímaussaq Complex, South Greenland. *Chem. Geol.* **258**, 65–77.
- Schuessler J. A., Schoenberg R. and Sigmarsson O. (2009) Iron and lithium isotope systematics of the Hekla volcano, Iceland – evidence for Fe isotope fractionation during magma differentiation. *Chem. Geol.* **258**, 78–91.
- Smith H. S. and Erlank A. J. (1982) Geochemistry and petrogenesis of komatiites from the Barberton greenstone belt, South Africa. In *Komatiites* (eds N. T. Arndt and E. G. Nisbet). Allen and Unwin, London, pp. 347–398.
- Sobolev A. V., Hofmann A. W., Kuzmin A. V., Yaxley G. M., Arndt N. T., Chung S.-L., Danyushevsky L. V., Elliott T., Frey F. A., Garcia M. O., Gurenko A. A., Kamenetsky V. S., Kerr A. C., Krivolutskaya N. A., Matvienkov V. V., Nikogosian I. K., Rocholl A., Sigurdsson I. A., Sushchevskaya N. M. and Teklay M. (2007) The amount of recycled crust in sources of mantle-derived melts. *Science* **316**, 412–417.
- Teng F.-Z., Wadhwa M. and Helz R. T. (2007) Investigation of magnesium isotope fractionation during basalt differentiation: implications for a chondritic composition of the terrestrial mantle. *Earth Planet. Sci. Lett.* **261**, 84–92.
- Teng F.-Z., Dauphas N. and Helz R.-T. (2008) Iron isotope fractionation during magmatic differentiation in Kilauea Iki lava lake. *Science* **320**, 1620–1622.
- Teng F.-Z., Ke S., Marty B., Dauphas N., Huang S., Pourmand A. (2010) The magnesium isotopic composition of the Earth and chondrites. *Lunar Planet. Sci. Conf.* **41**, #2019.
- Thompson A., Ruiz J., Chadwick O. A., Titus M. and Chorover J. (2007) Rayleigh fractionation of iron isotopes during pedogenesis along a climate sequence of Hawaiian basalt. *Chem. Geol.* **238**, 72–83.
- Tipper E. T., Louvat P., Capmas F., Galy A. and Gaillardet J. (2008) Accuracy of stable Mg and Ca isotope data obtained by MC-ICP-MS using the standard addition method. *Chem. Geol.* **257**, 65–75.
- Toplis M. J. (2005) The thermodynamics of iron and magnesium partitioning between olivine and liquid: criteria for assessing and predicting equilibrium in natural and experimental systems. *Contrib. Mineral. Petrol.* **149**, 22–39.
- Walker D., Jurewicz S. and Watson E. B. (1988) Adcumulus dunite growth in a laboratory thermal gradient. *Contrib. Mineral. Petrol.* **99**, 306–319.
- Watson E. B. and Baxter E. F. (2007) Frontiers: diffusion in the solid Earth. *Earth Planet. Sci. Lett.* **253**, 307–327.
- Watson E. B. and Müller T. (2009) Non-equilibrium isotopic and elemental fractionation during diffusion-controlled crystal growth under static and dynamic conditions. *Chem. Geol.* **267**, 111–124.
- Weyer S., Anbar A., Brey G. P., Münker C., Mezger K. and Woodland A. B. (2005) Iron isotope fractionation during planetary differentiation. *Earth Planet. Sci. Lett.* **240**, 251–264.
- Weyer S. and Ionov D. A. (2007) Partial melting and melt percolation in the mantle: the message from Fe isotopes. *Earth Planet. Sci. Lett.* **259**, 119–133.
- Weyer S., Anbar A., Brey G.P., Münker C., Mezger K. and Woodland A.B. (2007) Fe-isotope fractionation during partial melting on Earth and the current view on the Fe-isotope budgets of the planets (reply to the comment of F. Poitrasson and to the comment of B.L. Beard and C.M. Johnson on “Iron isotope fractionation during planetary differentiation” by S. Weyer, A.D. Anbar, G.P. Brey, C. Münker, K. Mezger and A.B. Woodland). *Earth Planet. Sci. Lett.* **256**, 638–646.
- Wiechert U. and Halliday A. N. (2007) Non-chondritic magnesium and the origins of the inner terrestrial planets. *Earth Planet. Sci. Lett.* **256**, 360–371.
- Wiederhold J. G., Kraemer S. M., Teutsch N., Borer P. M., Halliday A. N. and Kretzschmar R. (2006) Iron isotope fractionation during proton-promoted, ligand-controlled, and reductive dissolution of goethite. *Environ. Sci. Technol.* **40**, 3787–3793.
- Williams H. M., McCammon C. A., Peslier A. H., Halliday A. N., Teutsch N., Levasseur S. and Burg J.-P. (2004) Iron isotope fractionation and the oxygen fugacity of the mantle. *Science* **304**, 1656–1659.
- Williams H. M., Peslier A. H., McCammon C., Halliday A. N., Levasseur S., Teutsch N. and Burg J.-P. (2005) Systematic iron isotope variations in mantle rocks and minerals: the effects of partial melting and oxygen fugacity. *Earth Planet. Sci. Lett.* **235**, 435–452.
- Yang W., Teng F.-Z. and Zhang H.-F. (2009) Chondritic magnesium isotopic composition of the terrestrial mantle: a case study of peridotite xenoliths from the North China craton. *Earth Planet. Sci. Lett.* **288**, 475–482.
- Young E. D. and Galy A. (2004) The isotope geochemistry and cosmochemistry of magnesium. *Rev. Mineral. Geochem.* **55**, 197–230.